Silicon (2022) 14:1093–1121
https://doi.org/10.1007/s12633-020-00888-2

ORIGINAL PAPER

Abrasive Water Jet Machining of Al6063/B_4C/$ZrSiO_4$ Hybrid Composites: a Study of Machinability and Surface Characterization Analysis

P. Thamizhvalavan[1] · N. Yuvaraj[2] · S. Arivazhagan[3]

Received: 22 July 2020 / Accepted: 8 December 2020 / Published online: 6 January 2021

Abstract
This paper reports the machinability studies on aluminium hybrid composites of different compositions by using abrasive water jet machining process. In this study, aluminum hybrid metal matrix composites (HMMCs) with 5%, 10% and 15% Boron Carbide (B_4C) and 5% Zirconium Silicate ($ZrSiO_4$) with Al 6063 were fabricated using stir casting method. The cutting experiments were carried out by varying the water jet pressure, traverse rate, abrasive flow rate, and abrasive mesh size, and their effects on depth of cut (DOC), material removal rate (MRR) and surface roughness (R_a) were analyzed. Experiments were designed by using Box-Behnken response surface design, and the results were analyzed with response surface plots. In addition, the detailed surface evaluation studies were carried out by using 3D surface topography and morphology descriptions. Regression equations were developed to determine the significant factors in HMMCs. ANOVA test results were established for checking model adequacy in HMMCs with various responses. The results indicated that the proportion rate of B_4C with $ZrSiO_4$ ceramic particles in Al6063 affects the machinability and surface quality features. Also, the abrasive mesh size was found to be the responsible factors for higher DOC, MRR and lower R_a in HMMCs. The machined surface of hybrid composites shows the ploughing effect and cavities indicating both ductile and brittle fracture mechanisms.

Keywords Al6063 · B_4C · $ZrSiO_4$ · Abrasive water jet · Machinability · Morphology

1 Introduction

Hybrid metal matrix composite (HMMC) has the ability to fulfill the current demands of advanced engineering applications. Usually, HMMCs are mixtures of materials having a metal base with two ceramics, which show better mechanical properties such as stiffness, balanced bending and membrane, strength, reduced weight, improved fatigue resistance, improved damping capability and good shielding against nuclear radiation when compared with MMCs of single reinforcement [1, 2]. Among the various HMMCs, aluminium HMMCs are in high demand for enhanced mechanical properties and reduced weight with low production cost to different applications such as automobile, aerospace, marine, etc. [3]. In the recent days efforts have been taken to introduce various hard ceramic particulates like Zirconia, SiC, Al_2O_3, CNT, hBN and B_4C to the aluminum base matrix as reinforcements to increase the hardness and wear resistance properties [2, 4–6]. Compared to others, B_4C is an essential material for numerous fields, and is widely used in tank armor and nuclear radiation absorber due to its excellent ballistic properties where the aluminium metal matrix is a base material [7]. In addition, $ZrSiO_4$ is another type of the hard reinforcements used in HMMCs which is having the remarkable properties of high strength, hardness and wear resistance [8]. It also withstands high temperature and chemical reactions. Hard reinforcements in the aluminium metal matrix composites become hard and brittle, and these materials are more homogeneous and anisotropic in nature. However, the presence of hard reinforcements

✉ N. Yuvaraj
yuvaceg09@gmail.com

[1] Department of Mechanical Engineering, Jaya College of Engineering and Technology, Chennai 56, India

[2] Department of Mechanical Engineering, Vel Tech Rangarajan Dr. Sagunthala R&D Institute of Science and Technology, Chennai 62, India

[3] Department of Mechanical Engineering, St. Joseph's College of Engineering, Chennai 119, India

leads to poor machinability in conventional machining. As a result, the tool failure increases due to the presence of hard reinforcements which tends to wrap around the cutting tool bit leading to the tool breakage [9].

Researchers also studied the machinability of HMMCs/MMCs by using advanced machining operations. Karabulut et al. [7] have studied the machinability of Al6061/B_4C through an influence of weight fraction of B_4C particles in Al6061 by using wire electrical discharge machining (WEDM) process. The results indicate that a better surface finish was found in Al6061 reinforced with 15% of B_4C. Also, Sathiskumar et al. [10] have investigated the WEDM of Al6063/SiC MMC with varying amount of reinforcements. The results indicated that the recast layer was observed on aluminum, which is attributed to the influence of heat by WEDM. In addition, the Electro Chemical Machining process suits for composites, but it requires an improvised electrolytic concentration and electrolyte conductivity composites to achieve better surface finish [11]. Ravindra and Vinod [12] have investigated the machining of hybrid metal matrix composites using the Electrical Discharge Grinding process. The machined composite surface shows the recast layer and abrasive marks. Muller and Monaghan [13] studied the machining of Al/SiC using the Electrical Discharge Machining process. It is observed that the process resulted in crater like surface and the size of the crater increases with increase in discharged energy and sub-surface damage is relatively small. Pramanik [14] studied the machining of particle reinforced MMCs using laser cutting operation. Excessive heating in laser cutting melts and evaporates the matrix materials as well as reinforced particles. Due to the surface imperfections in the existing process, the cold machining technique like abrasive water jet machining process is established for machining HMMCs because of negligible heat generation, minimum induced stress, high machining versatility, high flexibility, small cutting forces, high productivity and better adaptability. In AWJ process, material removal takes place through the erosion principle and it is controlled by various process parameters. And, the process details are referred with Natarajan et al. [15].

The following discussion deals with AWJ machining of MMCs and HMMCs. Santhanakumar et al. [16] have investigated surface characteristics in AWJ cutting of Al6061/10%SiC/10%Al_2O_3 composites using the grey relation response surface method. A water pressure of 234.94 MPa, an abrasive flow rate of 103.41 g/min, a traverse speed of 91.54 mm/min and a standoff distance of 1.77 mm were found to be optimal parameters for a lower striation formation. Gnanavelbabu et al. [17] have investigated the cutting of Al6061/B_4C/hBN by AWJ. They reported that increase in B_4C (5 to 15%) increases the surface roughness and water jet pressure of 275 MPa reduces the taper angle. Kumar et al. [18] have studied the influence of AWJ process parameters in aluminum/ 2–10 wt% of tungsten carbide composites. The results reveal that MRR was highly influenced by traverse rate which is followed by percentage of reinforcement and SOD. Also, the decrement of surface roughness was observed with increment in weight percentage of tungsten carbide, traverse rate and SOD. Gnanavelbabu et al. [19] have investigated the effects of AWJ machining parameters on AA6061/B_4C/CNT. The reinforcement particles of 15% is found to improve the kerf taper angle under the influence of traverse speed and decrease in the reinforcement (from 15% to 5%) resulted in lower surface roughness (3.012 μm) under the significant parameters of pressure and traverse speed.

Srivastava et al. [20] have studied the surface integrity studies on AWJ turning of A359/2%B_4C/2%Al_2O_3. They have noticed the maximum MRR of 724 mm^3/min with rough surface of 8.6 μm was observed in the hybrid composite. The surface results also confirmed the ploughing nature of HMMC by the presence of undulated surface. It is also noticed that brittle fracture occurs in the region of hard reinforcement particles. Sasikumar et al. [21] studied on kerf characteristics of AWJ machining on hybrid aluminum 7075 metal matrix composites. It is found that with the increase in jet traverse speed from 30 to 90 mm/min, top kerf width and surface roughness decrease, whereas kerf angle increases. It is also suggested that water jet pressure of 280 MPa could be useful for better surface finish and minimum kerf angle.

Metin et al. [22] have predicted the surface roughness in AWJ of MMCs using genetic expression programming. The result reveals that the increase in the depth of cut from 3 to 33 mm increases the R_a, R_z and RSM values. The main mechanism of material removal was combination of scooping and plowing actions of the abrasives. Mardi et al. [23] have studied the machining of Mg based nano composites with the Al_2O_3 nano particle reinforcement of 0.66 weight percentage. A good surface finish and minimum sub-surface damage was obtained at a traverse speed of 20 mm/min, at a traverse speed of 500 mm/min micro melting was produced. Besides, the presence of abrasive particle embedded into metal matrix was observed. Srinivas and Babu [24] have investigated the penetration ability in Aluminum/SiC composites. The results indicate that contributions of water jet pressure and traverse speed are more on jet penetration than the abrasive flow rate. Ramulu et al. [25] have investigated the AWJ Characteristics of 30%vol SiC_P/Al6061-T6 and Al6061-T6 aluminum alloy composites. It is observed that with an increase in the angle of impact (5^o to 20^o), more damage and sub surface cracking was observed and the impacted specimen had deep craters on the surface. Hamatani and Ramulu [26] studied machinability of TiB_2/SiC and SiC/Al matrix composites. The experimental result reveals that good surface finish is achieved at a traverse rate of 50 mm/min, for both composites. Manoj et al. [27] have studied the machinability features of AWJ in Al

7075/TiB_2. It was found that water jet pressure had a great impact on surface roughness and material removal rate in AWJ cutting of aluminium composite components.

Neusen et al. [28] have investigated AWJ cutting of Aluminum silicon carbide and magnesium-based composites on increasing the abrasive flow rate decreased surface roughness also surface roughness increases with an increasing traverse speed and increase depth of cut decreases the traverse speed. Also, the abrasive wear by individual garnet particles appears to be one of the micro mechanisms of material removal in MMCs. Savrun et al. [29] have studied surface characteristics of SiC whisker/2124 aluminum and SiC whisker/Al_2O_3. The machined surface had relatively smooth surface with minimum sub surface microstructural damage. The micro hardness test on S_iCw/Al composites showed that AWJ does not work harden the surface. Kumaran et al. [30] investigated the effect of abrasive grain size on AA 6351/SiC/B_4C. The outcome of the study proved that coarse abrasive particle (#80) has a favorable effect on the MRR. Likewise, only with fine grain abrasive particles (#120) good surface finishing as well less taper are obtained. Srinivas and Babu [31] have studied the role of garnet and silicon carbide abrasives in AWJ cutting of Al/SiC MMC. The result reveals that use of 80 mesh size SiC abrasive results in higher depth of penetration. Yuvaraj and Kumar [32] have studied the cutting performance of AA5058-H32 aluminum alloy by using different abrasive mesh sizes. The results indicate that coarser abrasive (#80) has achieved a higher depth of penetration.

1.1 Research Gap

Hard reinforcements in the aluminium metal matrix composites become hard and brittle, and these materials are more homogeneous and anisotropic in nature. However, the presence of hard reinforcements leads to poor machinability in conventional machining. As a result, the tool failure increases due to the presence of hard reinforcements which tends to wrap around the cutting tool bit leading to the tool breakage. Also, the previous works have reported the existence of shearing, recast layer, pull out and microcracks over the machined surface through use of conventional and thermal based unconventional machining processes. Researchers have also attempted the AWJ technique in cutting of a few HMMC's. This results in better surface features comparable to the other machining operations. However, these studies were conducted with limited set of process parameters. Previous works also indicate that type of abrasives and mesh size play a significant role in AWJ machining performance for various materials.

Based on the review of available literature, it was found that the AWJ machining of Al6063 with the reinforcements of B_4C and $ZrSiO_4$ has not been reported. In the present work, machining of Al6063 and HMMCs with Al6063 reinforced with 5%, 10%, 15% B_4C keeping 5% $ZrSiO_4$in all the cases, using AWJ has been investigated. The garnet with different abrasive mesh size and various water jet pressure, abrasive flow rate and traverse rate, plays a vital role in achieving higher depth of cut, higher MRR and lower Ra. Performance analysis using RSM Box-Behnken design has been made in this work.

2 Materials and Methods

The following section explains about fabrication process of HMMCs, material characterization and experimental details.

2.1 Fabrication of HMMCs and its Characterization

Aluminum alloy (Al6063) is used as matrix material in the fabrication of HMMCs. Table 1 shows the chemical composition by weight percentages of Al6063 alloy. The elemental composition was made with optical emission spectrometer as per ASTM E125.

Figure 1 shows the fabrication set up for stir casting process for the fabrication of hybrid metal matrix composites using the reinforcement of B_4C (64 μm) and $ZrSiO_4$ (44 μm) with Al6063.Varied reinforcements were prepared at different weight percentages, such as 5%B_4C and 5%$ZrSiO_4$, 10%B_4C and 5%$ZrSiO_4$ and 15%B_4C and 5%$ZrSiO_4$ besides the unreinforced Al6063 through the stir casting process, in which an electrical fired crucible furnace was used to heat and melt the Al6063 at 750 °C followed by the pre heating of reinforcement of B_4C and $ZrSiO_4$ up to 800 °C for a period of 1 h in two different electrical furnaces. This was done for the removal of moisture. Also, to enhance the wet-ability of surface, the absorbed hydroxide and other gas was removed and 20 g of magnesium particles are added. The molten metal B_4C and $ZrSiO_4$ were mixed and stirred a speed of 300 rpm for 15 min.

During stir casting process 10 grams of degassing agent (hexachloro ethane) was added to molten metal for removing the slag. Once the prepared composites are obtained,

Table 1 Chemical composition of Al6063

Alloy	Si	Fe	Cu	Mn	Mg	Zn	Cr	Ni	V	Ti	Al
Al 6063	0.692	0.343	0.273	0.097	0.779	0.01	0.063	0.015	0.012	0.019	Balance

Fig. 1 Stir casting set up for HMMCs

they were poured into a die (trapezoidal shaped) to enable the cooling process at room temperature for a period of 3 h. Following this, the microstructures of HMMCs were obtained by using an optical microscope for the confirmation of distribution of reinforcements, and are shown in Fig. 2. The SEM images ofAl6063 alloy and Al6063/5%B_4C/5%$ZrSiO_4$, Al6063/10%B_4C/5%$ZrSiO_4$, Al6063/15%B_4C/5%$ZrSiO_4$ composites are presented in Fig. 3. From these results, the presence of B_4C (black spots) and $ZrSiO_4$ (white spots) particles in the fabricated HMMCs was confirmed. In addition, the reinforcement particles strengthen the grain boundaries by broadening it. Figure 4 also shows the element composition of Al6063 alloy and HMMCs. This result was obtained by using energy dispersive X-Ray spectroscopy (EDS). Besides, hardness was also measured at different locations on Al6063 and hybrid composites by using Vickers hardness tester with a load of 0.5 kg. The mean hardness values were found to be 46.95, 48.42, 48.95, and 49.11 respectively.

2.2 Experimental Setup

Cutting operations were carried out on trapezoidal shaped work pieces by using an injection type AWJM machining center as shown in Fig. 5. The work piece dimensions are shown in Fig. 6. A maximum pressure of 360 MPa and traverse speed of 90 m/min was employed during machining. The machine has a travel capacity of 3500 mm in 'X' axis and 1500 mm in 'Y' axis. The orifice of 0.35 mm diameter, focusing nozzle tube of 0.75 mm diameter, and jet impact angle of 90° were employed for cutting operations. Table 2 shows the process parameters and its levels. The experiments were designed by using response surface methodology with Box-Behnken design, and its experimental design layout is shown in Table 3. In this study, garnet abrasives with different mesh sizes were chosen for this study as shown in Fig. 7. It was confirmed that the size and shape of the grains were varied. The output parameters were considered in this study as depth of cut, material removal rate and surface roughness. The AWJ machined materials are shown in Fig. 8.

2.3 Measurement of Performance and Surface Responses

The following equations were used for the measurement of various responses considered in this study.

The depth of cut (DOC) was measured by the slant length of jet penetration and angle of the modified target material. The values were taken by using Eq. (1)

$$DOC = L * Sin25° \tag{1}$$

where, DOC – Depth of cut (mm); L – Length of cut (mm).

The material removal rate (MRR), mm^3/min was measured by using Eq. (2). It is the product of depth of penetration, average kerf width and traverse rate

$$MRR = DOC * KWavg * TR \tag{2}$$

where,

$$TR\text{–Traverse rate, } \left(\frac{mm}{min}\right); KWavg\text{–Average kerf width, (mm).}$$

Also, the measurement of surface roughness (R_a) was done by using Taylor Hobson Surtonic 3+ contact type portable stylus type profilometer with a cut off length of 0.8 mm and traverse length of 4 mm. This measurement was carried out in the traverse direction of machined surface and the measurement is repeated by three times for the average measurement of R_a. A non-contact 3D surface profiler (Talysurf CCI-Lite) was also employed for obtaining 2D roughness profile and 3D surface topography of the various machined surfaces.

Scanning electron microscope (Hitachi model S-3400 N) with a magnification of 500X and 1000X was taken for the

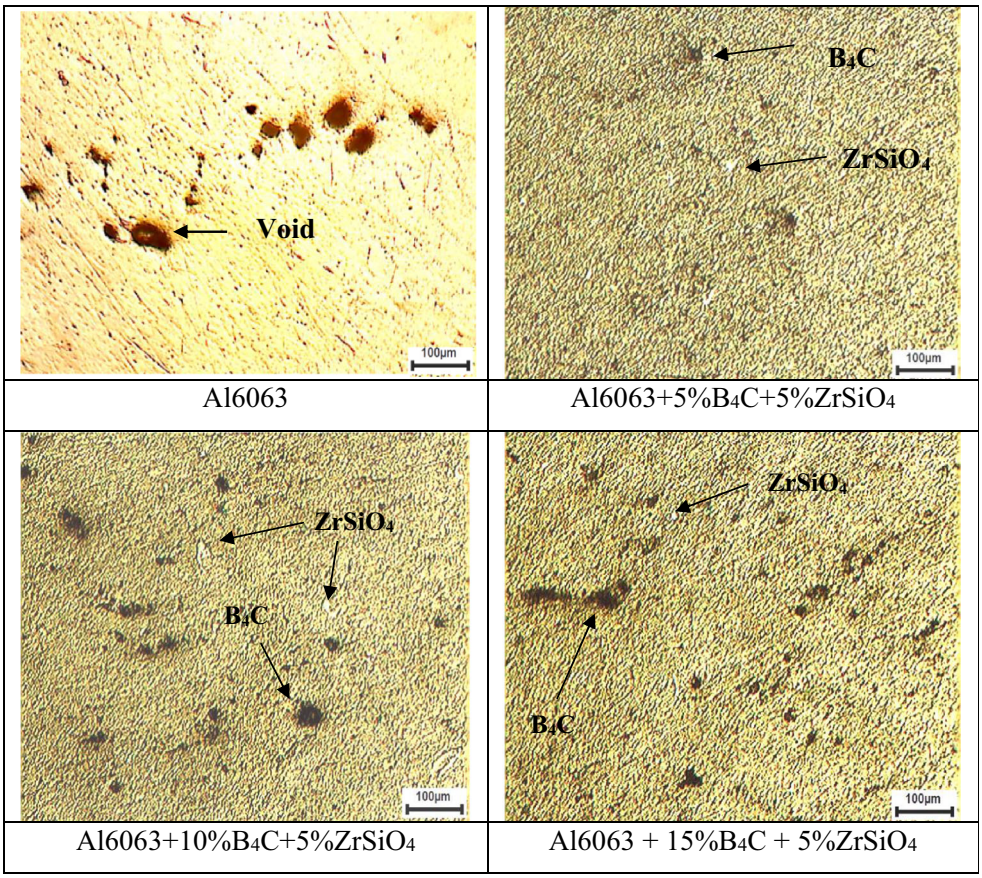

Fig. 2 Microscopic images of stir-casted HMMCs

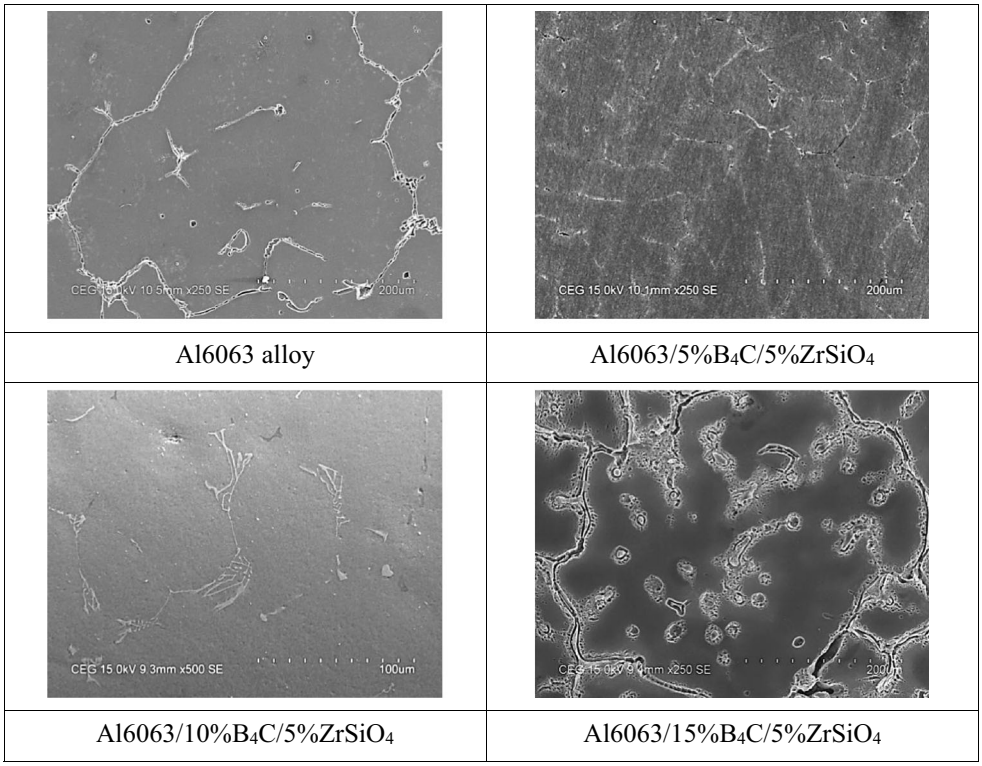

Fig. 3 SEM images of stir-casted HMMCs

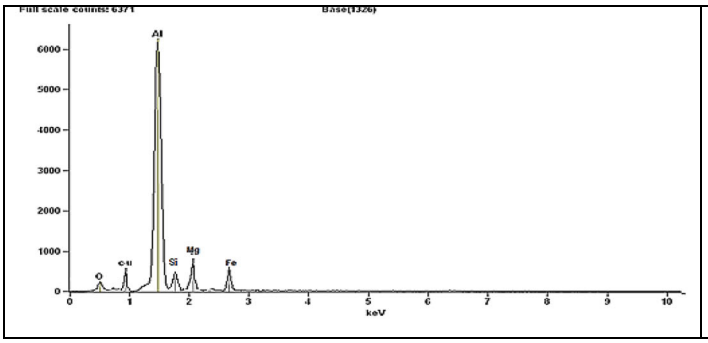

Elements	Weight %
O	0.27
Si	0.63
Mg	0.012
Cu	0.10
Fe	0.31
Al	98.678
Total	100.00

(a)

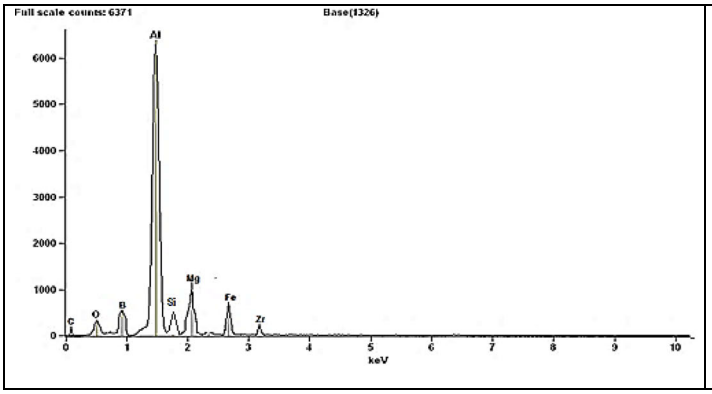

Elements	Weight %
C	0.95
O	4.81
Si	2.20
B	1.70
Mg	0.76
Zr	1.24
Al	88.20
Fe	0.14
Total	100.00

(b)

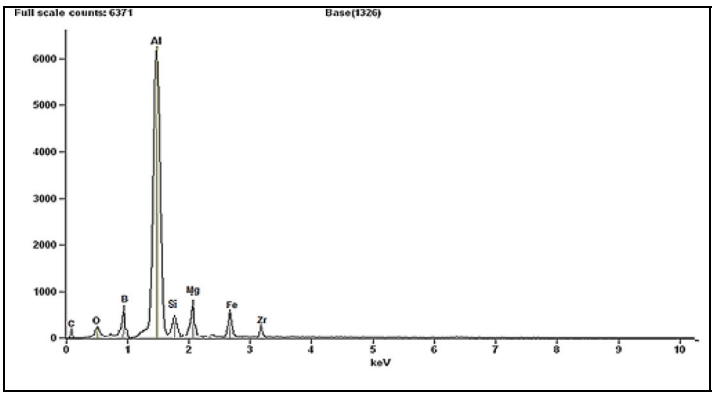

Elements	Weight %
C	0.47
O	3.77
Si	1.97
B	2.29
Mg	0.82
Zr	1.17
Fe	0.23
Al	89.28
Total	100.00

(c)

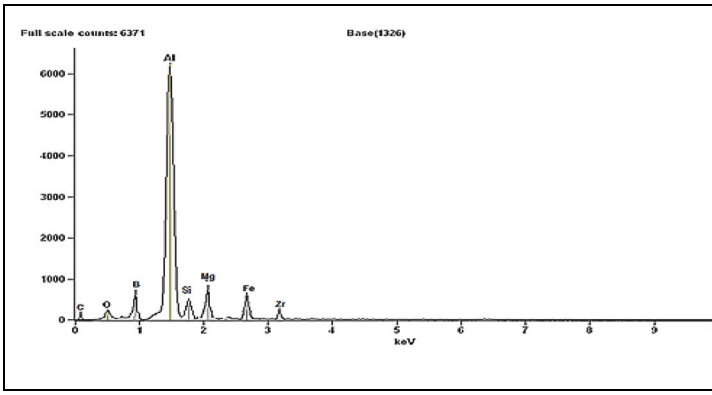

Elements	Weight %
C	0.21
O	3.17
Si	1.73
B	2.63
Mg	0.72
Zr	1.14
Fe	0.19
Al	90.21
Total	100.00

(d)

Fig. 4 Chemical composition of base material and HMMCs. **a** Al 6063 alloy **b** Al6063/5%B_4C/5%$ZrSiO_4$ **c** Al6063/10%B_4C/5%$ZrSiO_4$ **d** Al6063/15%B_4C/5%$ZrSiO_4$

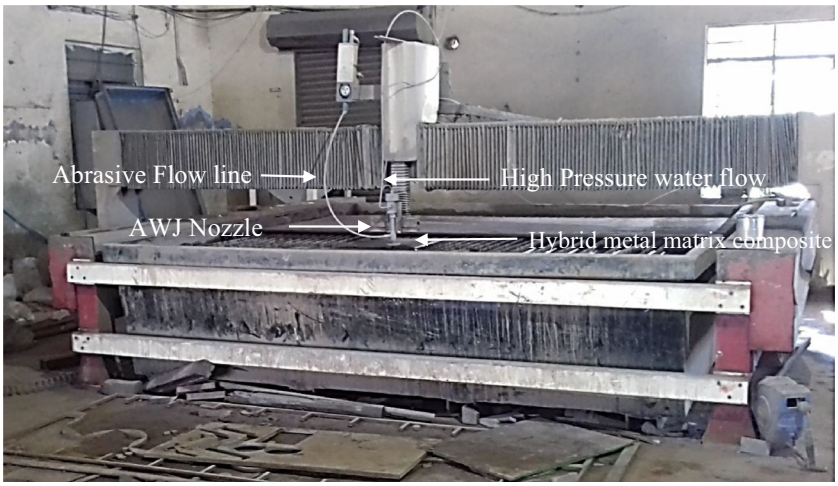

Fig. 5 AWJ machining centre

critical examination of surface morphology in AWJ machined surfaces. Also, the abrasive particle contamination was analyzed on the top cut surfaces by using energy dispersive X-Ray spectroscopy (EDS).

3 Results and Discussion

3.1 ANOVA and RSM for DOC on Different Materials

Tables 4, 5, 6 and 7 indicate the ANOVA results for the depth of cut for all materials. In this study, ANOVA was carried out to examine the model adequacy checking through RSM approach. From the results, it is observed that model *p* values of all materials confirmed that each model was statistically significant as its p value was less than 0.05. This confirms the variation in the responses. ANOVA test was conducted with 5% significance and 95% confidence intervals. Also, the lack of fit value was examined for the adequacy of various developed models. However, it is noticed that the significant level for the lack of fit of p value is less than 0.05. It can be viewed that the pure error of each model was lower than its residual error. This result was produced due to the formation of outliers in each developed model. It may develop due to the repetition in the experimental values of DOC.

As a consequence, the percentage of R-values was decreased to 85.57%, 82.8%, 82.4%, and 82.84% for Al6063, Al6063/5%B_4C/5%$ZrSiO_4$, Al6063/10%B_4C/5%$ZrSiO_4$, and Al6063/15%B_4C/5%$ZrSiO_4$ respectively. This result is further confirmed by the presence of outliers and distribution of residues in the developed models, and is shown in Fig. 9. It is highlighted by red color in predicted vs. actual plots. It can be also found that residues were closer to the straight line representing that the model is accurate. Outliers might be reduced by decreasing the value of residual error than pure error. Further, it can be obtained by the selection of narrow range of process parameters for HMMCs. Despite this, the process parameters were considered after the trial and error runs were carried out. However, the levels of process parameters further need to be optimized by the consideration of hard reinforcement particles in Al6063 alloy.

In this study, the response surface methodology was used for correlating the output responses with cutting parameters so as to estimate the effects of process parameters (water jet pressure, abrasive flow rate, traverse rate, and abrasive mesh size) on DOC. In this regard, the second order quadratic models of DOC were developed with four

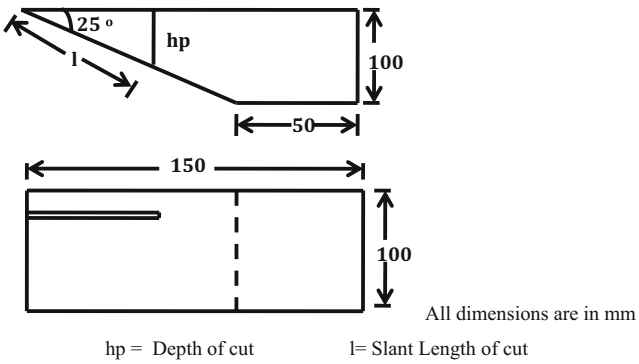

Fig. 6 Trapezoidal work piece

Table 2 Process parameters of AWJ

Process parameters	Level 1	Level 2	Level 3
Water jet pressure, (MPa)	125	200	275
Traverse rate, (mm/min)	60	90	120
Abrasive flow rate, (g/min)	240	340	440
Abrasive mesh size, (#)	80	100	120

Table 3 Box-Behnken design (L_{29}) for AWJ cutting experiments

Exp. No.	Process parameters			
	Water jet pressure, MPa	Traverse rate, mm/min	Abrasive flow rate, g/min	Abrasive mesh size, #
1	125	60	340	100
2	275	60	340	100
3	125	120	340	100
4	275	120	340	100
5	200	90	240	80
6	200	90	440	80
7	200	90	240	120
8	200	90	440	120
9	125	90	340	80
10	275	90	340	80
11	125	90	340	120
12	275	90	340	120
13	200	60	240	100
14	200	120	240	100
15	200	60	440	100
16	200	120	440	100
17	125	90	240	100
18	275	90	240	100
19	125	90	440	100
20	275	90	440	100
21	200	60	340	80
22	200	120	340	80
23	200	60	340	120
24	200	120	340	120
25	200	90	340	100
26	200	90	340	100
27	200	90	340	100
28	200	90	340	100
29	200	90	340	100

experimental parameters. Response surface models were used to determine the AWJ significant factor for Al6063 alloy and its hybrid composites. The response surface models are shown in Eqs. (3) to (6).

3.1.1 Model Equation for Al 6063 Alloy

$$\begin{aligned}\mathrm{DOC} = {} & +14.91304-(0.00624*\mathrm{WP})-(0.040683*\mathrm{TR}) \\ & +(0.00515*\mathrm{AFR})-(0.19050*\mathrm{AMS}) \\ & +(0.000030*\mathrm{WP}*\mathrm{TR})-(0.00000033*\mathrm{WP}*\mathrm{AFR}) \\ & -(0.00000833*\mathrm{WP}*\mathrm{AMS})-(0.00000750*\mathrm{TR}*\mathrm{AFR}) \\ & +(0.0001833*\mathrm{TR}*\mathrm{AMS}) \\ & +(0.000025*\mathrm{AFR}*\mathrm{AMS}) \\ & +\left(0.0000108*\mathrm{WP}^2\right) \\ & +\left(0.000088*\mathrm{TR}^2\right)-\left(0.0000098*\mathrm{AFR}^2\right) \\ & +\left(0.000714*\mathrm{AMS}^2\right)\end{aligned} \tag{3}$$

3.1.2 Model Equation for Al6063 + 5%B_4C + 5%$ZrSiO_4$

$$\begin{aligned}\mathrm{DOC} = {} & +69.86304-(0.18916*\mathrm{WP})-(0.21144*\mathrm{TR}) \\ & +(0.045253*\mathrm{AFR})-(0.44225*\mathrm{AMS}) \\ & +(0.000400*\mathrm{WP}*\mathrm{TR}) \\ & +(0.000033*\mathrm{WP}*\mathrm{AFR}) \\ & +(0.00178*\mathrm{WP}*\mathrm{AMS})+(0.00033*\mathrm{TR}*\mathrm{AFR}) \\ & +(0.000458*\mathrm{TR}*\mathrm{AMS}) \\ & +(0.00033*\mathrm{AFR}*\mathrm{AMS})-\left(0.000216*\mathrm{WP}^2\right) \\ & -\left(0.000100*\mathrm{TR}^2\right)-\left(0.000156*\mathrm{AFR}^2\right) \\ & -\left(0.00128*\mathrm{AMS}^2\right)\end{aligned} \tag{4}$$

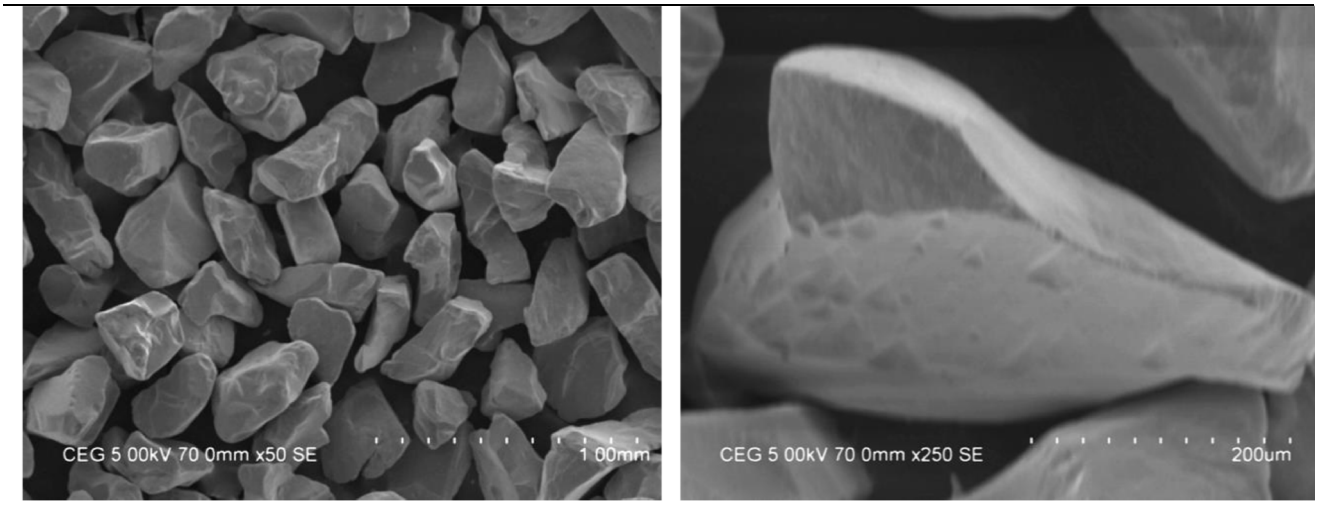

(a)

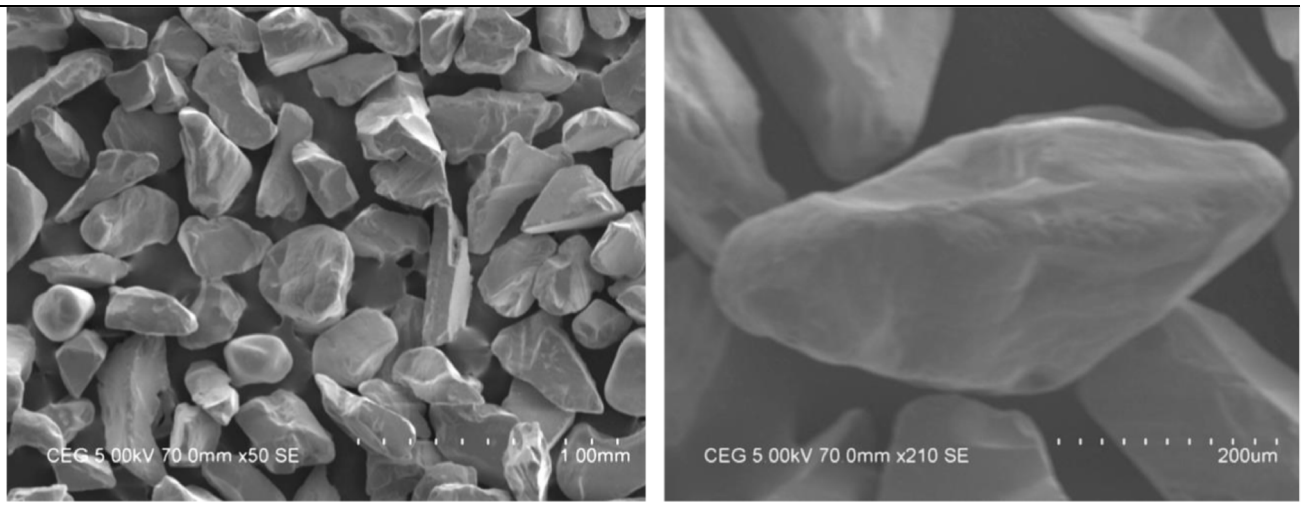

(b)

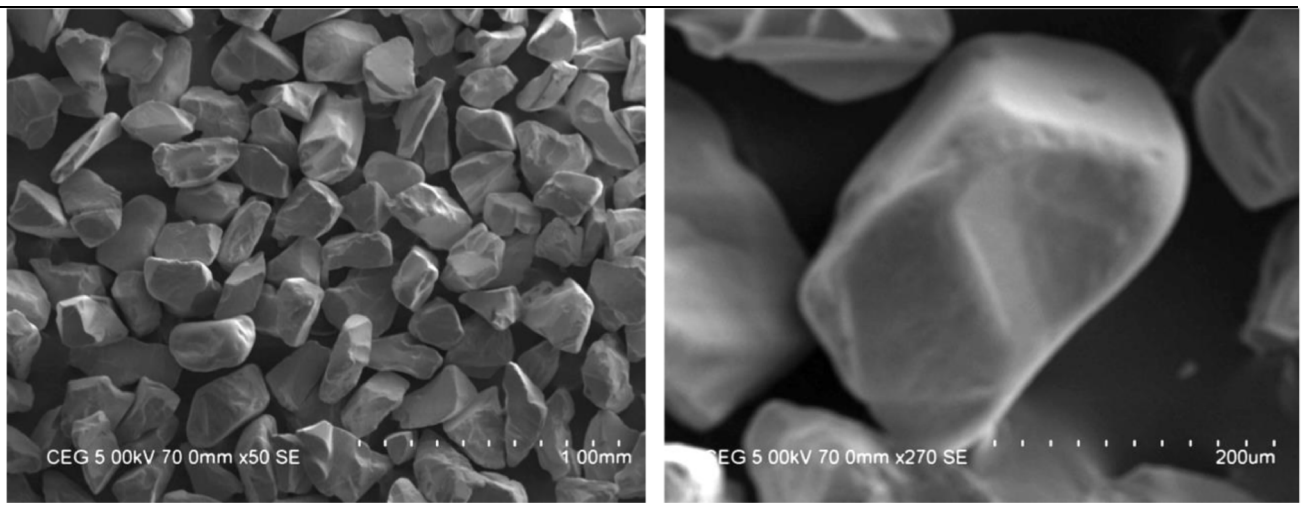

(c)

Fig. 7 Garnet abrasive with different mesh sizes. **a** Garnet mesh size #80 **b** Garnet mesh size #100 **c** Garnet mesh size #120

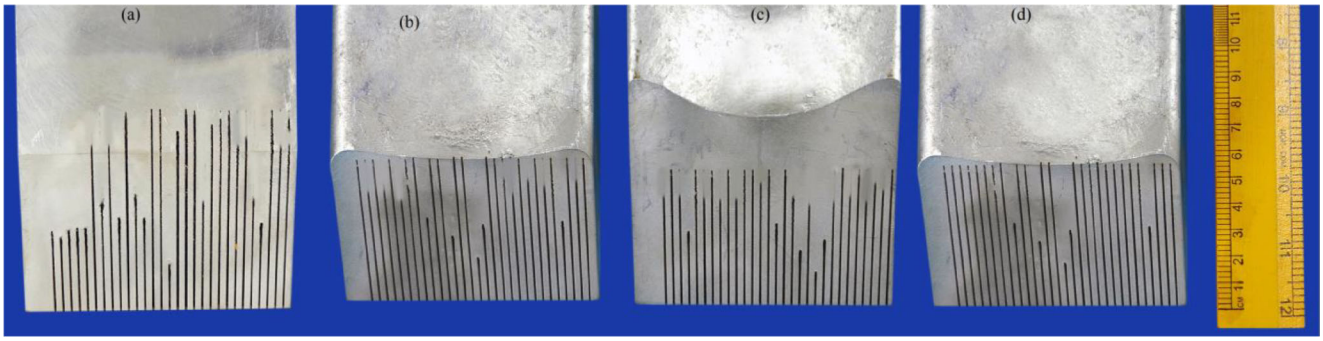

Fig. 8 AWJ machined materials (**a**) Al6063 alloy (**b**) Al6063/5%B_4C/5%$ZrSiO_4$(**c**) Al6063/10%B_4C/5%$ZrSiO_4$(d) Al6063/15%B_4C/5%$ZrSiO_4$

Model Equation for Al6063 + 10%B_4C + 5%$ZrSiO_4$

$$\begin{aligned}\mathrm{DOC} = {} & +39.99730-(0.19093*\mathrm{WP})-(0.23621*\mathrm{TR}) \\ & +(0.10688*\mathrm{AFR})-(0.092042*\mathrm{AMS}) \\ & +(0.0005011*\mathrm{WP}*\mathrm{TR}) \\ & +(0.0000086*\mathrm{WP}*\mathrm{AFR}) \\ & +(0.001401*\mathrm{WP}*\mathrm{AMS}) \\ & +(0.00017*\mathrm{TR}*\mathrm{AFR}) \\ & +(0.000216*\mathrm{TR}*\mathrm{AMS}) \\ & +(0.00003125*\mathrm{AFR}*\mathrm{AMS})-(0.0001096*\mathrm{WP}^2) \\ & +(0.000340*\mathrm{TR}^2)-(0.0001719*\mathrm{AFR}^2) \\ & -(0.00189*\mathrm{AMS}^2)\end{aligned} \tag{5}$$

3.1.3 Model Equation for Al6063 + 15%B_4C + 5%$ZrSiO_4$

$$\begin{aligned}\mathrm{DOC} = {} & +51.93797-(0.15513*\mathrm{WP})-(0.075556*\mathrm{TR}) \\ & +(0.042425*\mathrm{AFR})-(0.43067*\mathrm{AMS}) \\ & -(0.00159*\mathrm{WP}*\mathrm{TR}) \\ & +(0.0000166*\mathrm{WP}*\mathrm{AFR}) \\ & +(0.000152*\mathrm{WP}*\mathrm{AMS}) \\ & +(0.000208*\mathrm{TR}*\mathrm{AFR}) \\ & +(0.000137*\mathrm{TR}*\mathrm{AMS}) \\ & +(0.0000375*\mathrm{AFR}*\mathrm{AMS})-(0.000084*\mathrm{WP}^2) \\ & +(0.000216*\mathrm{TR}^2)-(0.0000868*\mathrm{AFR}^2) \\ & -(0.00010*\mathrm{AMS}^2)\end{aligned} \tag{6}$$

3.2 Influence of Parameters on Al6063 Alloy and its Hybrid Composites for DOC

Figure 10 shows the interaction of significant process parameters in Al6063 and their hybrid metal matrix composites. The significant process parameters were found by using regression Eqs. (3) to (6). The interaction parameters were selected based on the higher co-efficient values in each type of material regression equation. From these results, it is observed that depth of cut is significantly influenced by the interaction between abrasive mesh sizes and traverse rates for all materials except Al6063 reinforced with 15% of B_4C and 5% $ZrSiO_4$. The influencing process parameters combinations were composed from response surface plots based on higher DOC, and the results are shown in Table 8. From Table 8, it is found that the process parameters combinations remain same for all type of materials. This attainment was found at water jet pressure of 125 MPa, traverse rate of 120 mm/min, abrasive flow rate of 340 g/min and abrasive mesh size of #80.

Decrease in abrasive mesh size from # 120 to #80 increases the DOC up to 23.90 mm. This result was found due to the fact of that the larger size abrasive (~190 μm/#80) possess a critical cutting energy with a water jet pressure of 125 MPa and abrasive flow rate of 340 g/min were employed; as a result of this, uniform jet velocity is obtained. By maintaining a uniform velocity of water jet, produced a deeper penetration is produced thereby resulting in a higher DOC and is found to be 23.90 mm. It is attributed to the effect of lower water jet pressure was employed [29]. This range of pressure restricts the severe particle fracture in the cutting zone and mixing chamber which in turn to maintain the jet velocity while passing through the focusing nozzle; as a result, jet penetration depth was increased. In addition, the increase in traverse rate from 60 mm/min to 120 mm/min increases the depth of cut (Fig. 10a-c).

It is also noticed that increment in reinforcement percentage in Al6063 leads to decreases the depth of cut. This result is found due to the decrement in erosion rate by hard reinforcement particles in the matrix phase. It

Table 4 ANOVA for response surface quadratic model of DOC - Al6063

Source	Sum of Squares	Dof	Mean Square	F Value	*p* value Prob > F
Model	453.5	14	32.39	5.93	0.001
Residual	76.45	14	5.46		
Lack of Fit	76.3	10	7.63	206.32	< 0.0001
Pure Error	0.15	4	0.037		
Cor Total	529.95	28			
Std. Dev.	2.34	R-Squared	0.8557		
Mean	14.39	Adj R-Squared	0.7115		
C.V. %	16.23	Pred R-Squared	0.1703		
PRESS	439.71	Adeq Precision	10.266		

occurs due to the increment in hardness of the composites. Reinforcement particles such as B_4C and $ZrSiO_4$ restrict the jet penetration thereby resulting in lower penetration depth found in those materials. This consequence happens due to particle comminution takes place while cutting hard reinforcements in the material. The particle fracture and embedment in the reinforced particle pull out surface further reduces the jet penetration capability thereby resulting in lower depth of cut was found in hybrid composites compared to Al6063 alloy. A lowest depth of cut was noticed at 15% of B_4C and 5% of $ZrSiO_4$ in Al6063 and is found to be 5.3 mm. During machining of this composite, more abrasive particles getting fragmented which further reduce the jet penetration depth and also deflect the axis of the jet penetration from 90°. In this type of hybrid composite, the higher DOC was observed by varying the abrasive mesh size and traverse rate at a water jet pressure of 125 MPa and abrasive flow rate of 340 g/min. Increase in traverse rate from 60 mm/min to 120 mm/min with abrasive mesh size of #80, increases the intermolecular forces and energy thereby directing to strong shear surface and continuous erosion process in the particle reinforced composites. As a result, jet penetration depth was increased.

Compared to other materials, 15% of B_4C contributed a higher hardness to the matrix phase which demands the huge cutting energy for the production of higher DOC. This destructive action was accomplished through a significant involvement of process parameters combination which results in higher kinetic energy of the jet. The combined influencing action of abrasive mesh size with water jet pressure provides an adequate cutting energy for machining HMMCs with an enrichment of reinforcements. It is also observed that a slight variation in the DOC was found in all materials. This outcome has happened through the selection of level of process parameter settings in AWJ.

3.3 ANOVA and RSM for MRR on Different Materials

Tables 9, 10, 11 and 12 give that ANOVA results of Al 6063 alloy and its composites for MRR. It is noticed that all materials models had statistically significant, which is confirmed by *p* values (< 0.05). It can be also inferred that the lack of fit of different materials showed a significant as

Table 5 ANOVA for response surface quadratic model of DOC-Al6063 + 5%B_4C + 5%$ZrSiO_4$

Source	Sum of Squares	Dof	Mean Square	F Value	*p* value Prob > F
Model	409.18	14	29.23	4.8	0.0029
Residual	85.16	14	6.08		
Lack of Fit	84.66	10	8.47	66.64	0.0005
Pure Error	0.51	4	0.13		
Cor Total	494.34	28			
Std. Dev.	2.46	R-Squared	0.828		
Mean	13.28	Adj R-Squared	0.6559		
C.V. %	18.53	Pred R-Squared	0.0135		
PRESS	486.19	Adeq Precision	9.11		

Table 6 ANOVA for response surface quadratic model of DOC - Al6063 + 10%B_4C + 5%$ZrSiO_4$

Source	Sum of Squares	Dof	Mean Square	F Value	p value Prob > F
Model	331.55	14	23.68	4.68	0.0033
Residual	70.83	14	5.06		
Lack of Fit	70.61	10	7.06	128.11	0.0001
Pure Error	0.22	4	0.055		
Cor Total	402.39	28			
Std. Dev.	2.25	R-Squared	0.824		
Mean	12.16	Adj R-Squared	0.6479		
C.V. %	18.51	Pred R-Squared	−0.012		
PRESS	407.08	Adeq Precision	8.887		

lesser than 0.05. The p value of lack of fit is greater than 0.05 representing that residual error was decreased which is lesser than pure error. As a consequence, the model detects the lack of fit through a variation in response, and also confirms that the process parameters and the levels were suitable for that hybrid composite. Also, the residues follow the straight line, as shown in Fig. 11. Similar to DOC, few residues of MRR (outliers) located slightly far away from the straight line. Cluster forms of residues were also seen in predicted vs. actual plots. This formation occurs due to the lack of response of MRR even though parameter combinations were varied.

Similar to DOC, RSM was employed to relate the MRR with AWJ process parameters. For this, the second order quadratic models were developed in this study. The developed models were used to determine the significant factors for MRR on Al6063 alloy and its hybrid composites. The response surface models are given by Eqs. (7) to (10).

3.3.1 Model Equation for Al 6063 Alloy

$$\begin{aligned}\mathrm{MRR} = {} & +3258.07461-(9.26213*\mathrm{WP})+(9.93662*\mathrm{TR})\\ & +(4.18518*\mathrm{AFR})-(41.37488*\mathrm{AMS})\\ & -(0.011650*\mathrm{WP}*\mathrm{TR})-(0.0040275*\mathrm{WP}*\mathrm{AFR})\\ & +(0.14861*\mathrm{WP}*\mathrm{AMS})\\ & +(0.020963*\mathrm{TR}*\mathrm{AFR})\\ & +(0.010875*\mathrm{TR}*\mathrm{AMS})\\ & +(0.016622*\mathrm{AFR}*\mathrm{AMS})-(0.015706*\mathrm{WP}^2)\\ & -(0.031035*\mathrm{TR}^2)-(0.00903694*\mathrm{AFR}^2)\\ & -(0.040439*\mathrm{AMS}^2)\end{aligned} \tag{7}$$

3.3.2 Model Equation for Al6063 + 5%B_4C + 5%$ZrSiO_4$

$$\begin{aligned}\mathrm{MRR} = {} & +2527.57808-(7.20633*\mathrm{WP})+(6.76750*\mathrm{TR})\\ & +(1.98082*\mathrm{AFR})-(22.36238*\mathrm{AMS})\\ & -(0.006*\mathrm{WP}*\mathrm{TR})+(0.00225*\mathrm{WP}*\mathrm{AFR})\\ & +(0.12038*\mathrm{WP}*\mathrm{AMS})\\ & +(0.028875*\mathrm{TR}*\mathrm{AFR})\\ & +(0.067875*\mathrm{TR}*\mathrm{AMS})\\ & -(0.011644*\mathrm{AFR}*\mathrm{AMS})-(0.020097*\mathrm{WP}^2)\\ & -(0.073542*\mathrm{TR2})-(0.00431812*\mathrm{AFR}^2)\\ & -(0.079406*\mathrm{AMS}^2)\end{aligned} \tag{8}$$

3.3.3 Model Equation for Al6063 + 10%B_4C + 5%$ZrSiO_4$

$$\begin{aligned}\mathrm{MRR} = {} & +3457.43138+(6.85997*\mathrm{WP})\\ & +(28.21363*\mathrm{TR})\\ & +(3.07165*\mathrm{AFR})-(88.12444*\mathrm{AMS})\\ & +(0.00615*\mathrm{WP}*\mathrm{TR})\\ & +(0.000585*\mathrm{WP}*\mathrm{AFR})-(0.028012*\mathrm{WP}*\mathrm{AMS})\\ & -(0.0000375*\mathrm{TR}*\mathrm{AFR})-(0.005625*\mathrm{TR}*\mathrm{AMS})\\ & +(0.017212*\mathrm{AFR}*\mathrm{AMS})-(0.014725*\mathrm{WP}^2)\\ & -(0.12169*\mathrm{TR}^2)-(0.00659231*\mathrm{AFR}^2)\\ & +(0.35108*\mathrm{AMS}^2)\end{aligned} \tag{9}$$

Table 7 ANOVA for response surface quadratic model of DOC-Al6063 + 15%B_4C + 5%$ZrSiO_4$

Source	Sum of Squares	Dof	Mean Square	F Value	*p* value Prob > F
Model	247.73	14	17.7	4.83	0.0029
Residual	51.32	14	3.67		
Lack of Fit	50.37	10	5.04	21.16	0.0049
Pure Error	0.95	4	0.24		
Cor Total	299.06	28			
Std. Dev.	1.91	R-Squared	0.8284		
Mean	10.05	Adj R-Squared	0.6568		
C.V. %	19.05	Pred R-Squared	0.0249		
PRESS	291.62	Adeq Precision	9.635		

3.3.4 Model Equation for Al6063 + 15%B_4C + 5%$ZrSiO_4$

$$\begin{aligned} MRR = {} & +1908.22350-(0.41100*WP) \\ & +(21.44175*TR) \\ & +(6.20707*AFR)-(55.71000*AMS) \\ & +(0.00935*WP*TR) \\ & +(0.001125*WP*AFR)-(0.00585*WP*AMS) \\ & -(0.008325*TR*AFR) \\ & +(0.023813*TR*AMS) \\ & +(0.00253125*AFR*AMS)-\left(0.0045*WP^2\right) \\ & -\left(0.097125*TR^2\right)-\left(0.00824625*AFR^2\right) \\ & +\left(0.21628*AMS^2\right) \end{aligned} \quad (10)$$

3.4 Influence of Parameters on Al6063 Alloy and its Hybrid Composites for MRR

The influential factors were obtained from regression Eqs. (7)–(10). From these equations, it is noticed that abrasive mesh size and abrasive flow rate for Al 6063 alloy, abrasive mesh size and traverse rate for Al6063/5%B_4C/5%$ZrSiO_4$, Al6063/10%B_4C/5%$ZrSiO_4$ and Al6063/15%B_4C/5%$ZrSiO_4$. The interaction effects of these parameters on MRR with different materials are shown in Fig. 12. It indicates that process parameters combinations were varied for all materials. Similarly, the influencing factors combinations were obtained from the response surface plots and their results are given in Table 13. It is noticed that abrasive mesh size and traverse rate were the most influencing factors for increasing MRR for machining hybrid composite in which more than 10% of B_4C. This result produced due to the increment in hardness of the material by two hard reinforcements. It is also confirmed that abrasive mesh size #80 was found suitable to all materials for increasing MRR as these abrasives encompass higher density and coarse edges. These properties increase the cutting energy of abrasives compared to the other mesh sizes which results in higher MRR in all work materials and is observed to be in the range of 1140 to 1670 mm^3/min.

From Table 13, it is noted that a higher MRR was observed in Al6063 alloy followed by 5%B_4C/ 5%$ZrSiO_4$, 10%B_4C/ 5%$ZrSiO_4$, and 15%B_4C/ 5%$ZrSiO_4$. A soft nature of Al 6063 alloy allows the ductile erosion process more effectively, which results in higher MRR (1670 mm^3/min) being produced. This type of erosion process was confirmed through a presence of ploughing effect on the machined surface, as shown in Fig. 13. It can be observed that severe erosion (deformation of material) was seen in Al6063 alloy compared to the hybrid composite as shown in Fig. 14. From these results, it is also observed that abrasive mesh size and traverse rate were found as the influencing factors for the aluminium hybrid composites. This was happened that the intermolecular forces and cutting energy were increased by increasing traverse rate (60 mm/min to 120 mm/min) for machining HMMCs.

In Al6063 hybrid composites, by increasing reinforcement particles in the base material decreases the MRR. It can be attributed to the effect of hard reinforcement particles reduces the cutting energy of AWJ through its hardness, wear resistance and transformation of erosion mechanism from ductile to brittle fracture; as a result, MRR was decreased in all hybrid composites and a lowest MRR is observed to be 238 mm^3/min at Al6063/15%B_4C/5%$ZrSiO_4$. Also, no appreciable deformation was seen in Fig. 14. In addition, the interactions between

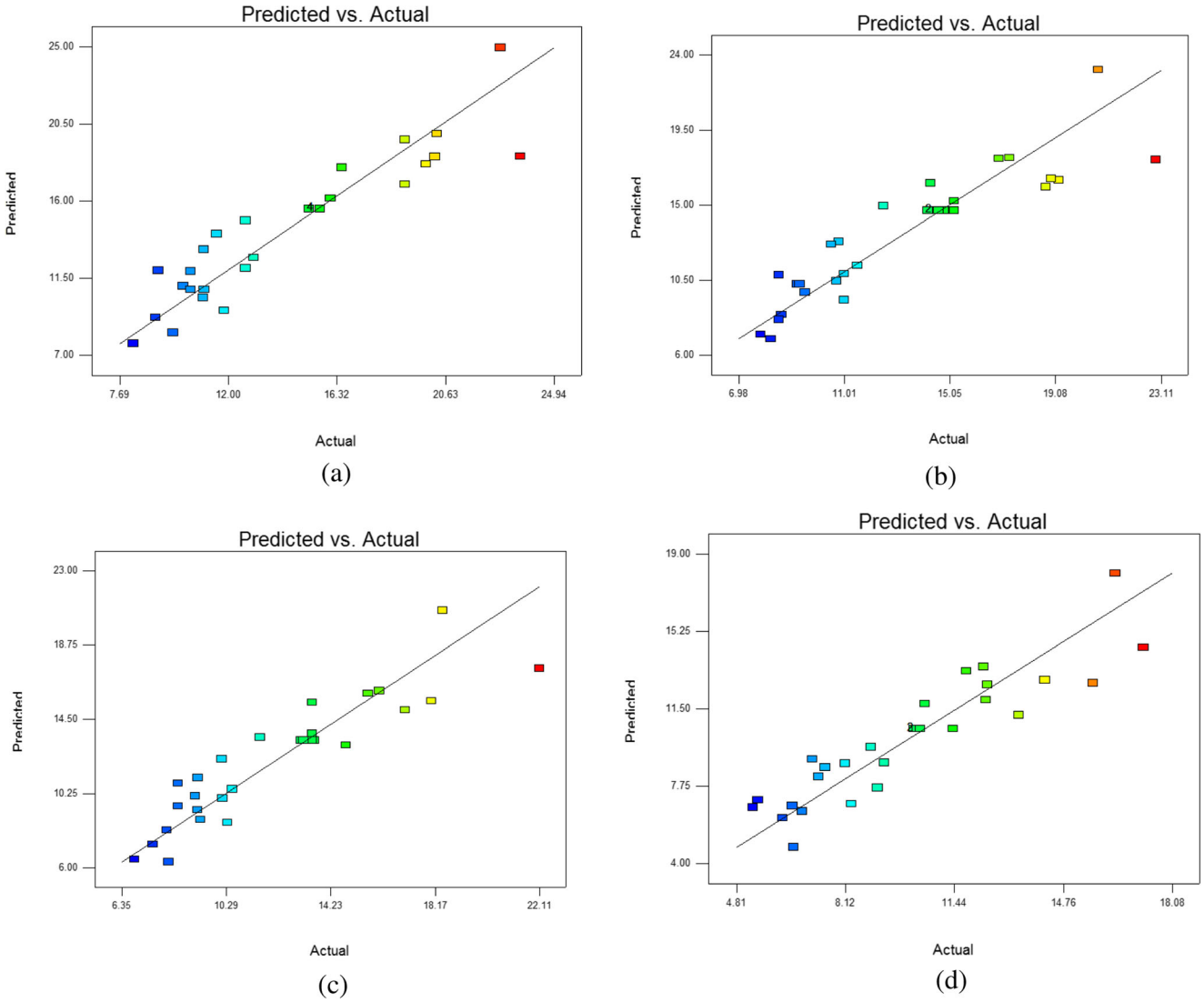

Fig. 9 Comparison between predicted and experimental values. **a** Al6063 **b** Al6063 + 5%B_4C + 5%$ZrSiO_4$ **c** Al6063 + 10%B_4C + 5%$ZrSiO_4$ **d** Al6063 + 15%B_4C + 5%$ZrSiO_4$

the reinforcement and garnet particles in the cutting zone could not allow the erosion process more effectively even though coarse abrasives (#80) were used. This ineffectiveness is happened owing to the occurrence of abrasive fracture (Fig. 14) by striking with the hard reinforcement particles. Due to the increment in wear resistance of the composites, material removal is deeply affected by the erosion process. In Al6063/15%B_4C/5%$ZrSiO_4$, it can be also viewed that an increment in erosion rate was observed at the water jet pressure of 125 MPa, traverse rate of 120 mm/min, abrasive flow rate of 340 g/min, and mesh size of #80. This low pressure allows the water jet with less deflection by decrement in particle fracture at the cutting zone and focusing nozzle. In addition, by the employment of moderate flow of coarse abrasives (340 g/min) with a traverse rate of 120 mm/min produced a stable cutting action, which helps to increase the MRR in Al6063/15%B_4C/5%$ZrSiO_4$.

3.5 ANOVA and RSM for R_a on Different Materials

Tables 14, 15, 16 and 17 give that ANOVA results for surface roughness (R_a) on AWJ machined surfaces for different materials. From these tables, it is noted that all materials models had statistically significant, which is confirmed by *p* values as less than 0.05. In addition, the p values of lack of fit showed no significance in Al6063 alloy and Al6063/10%B_4C/5%$ZrSiO_4$. This result confirms that the variation in surface roughness purely depends on AWJ cutting process parameters as their p values were greater than 0.05. It can be attributed that p value of residual error was lower than pure error. However, the process parameters were not appropriate for Al6063/10%B_4C/5%$ZrSiO_4$ and Al6063/15%B_4C/5%$ZrSiO_4$. It is happened due to the drastic changes in material properties through an inclusion of hard

reinforcements more than 5%. This may lead to act as an independent of surface roughness even though process parameters were varied. As a consequence, a repeatable error was observed, and is confirmed by predicted vs. actual values plots shown in Fig. 15. It is further confirmed by a formation of clusters in the residual plots. Outliers were also observed in Al6063/10%B_4C/5%$ZrSiO_4$ and Al6063/15%B_4C/5%$ZrSiO_4$. From the results, it can be concluded that the present selection of AWJ cutting parameters becomes ineffective while increasing reinforcement volume in the matrix phase.

The second order quadratic models were developed for surface roughness by using response surface methodology. The higher co-efficient values indicates that influencing factors for surface roughness on different materials. Influence factors were varied depends on the machined materials surface features. The model equations are given by;

3.5.1 Model Equation for Al 6063 Alloy

$$\begin{aligned} R_a = {} & +63.57907-(0.16088*\mathrm{WP})-(0.19926*\mathrm{TR}) \\ & +(0.10558*\mathrm{AFR})-(0.56093*\mathrm{AMS}) \\ & +(0.000177*\mathrm{WP}*\mathrm{TR})-(0.000059*\mathrm{WP}*\mathrm{AFR}) \\ & +(0.001868*\mathrm{WP}*\mathrm{AMS}) \\ & +(0.000211*\mathrm{TR}*\mathrm{AFR})+(0.00038*\mathrm{TR}*\mathrm{AMS}) \\ & +(0.000246*\mathrm{AFR}*\mathrm{AMS})-\left(0.000178*\mathrm{WP}^2\right) \\ & +\left(0.00037*\mathrm{TR}^2\right)-\left(0.000185*\mathrm{AFR}^2\right) \\ & -\left(0.000691*\mathrm{AMS}^2\right) \end{aligned} \tag{11}$$

3.5.2 Model Equation for Al6063 + 5%B_4C + 5%$ZrSiO_4$

$$\begin{aligned} R_a = {} & +12.96735+(0.00027*\mathrm{WP})+(0.00276*\mathrm{TR}) \\ & +(0.00867*\mathrm{AFR})-(0.19501*\mathrm{AMS}) \\ & +(0.000021*\mathrm{WP}*\mathrm{TR})-(0.00000043*\mathrm{WP}*\mathrm{AFR}) \\ & +(0.0000740*\mathrm{WP}*\mathrm{AMS}) \\ & +(0.0000627*\mathrm{TR}*\mathrm{AFR})-(0.0000745*\mathrm{TR}*\mathrm{AMS}) \\ & -(0.0000237*\mathrm{AFR}*\mathrm{AMS})-\left(0.0000238*\mathrm{WP}^2\right) \\ & -\left(0.000100*\mathrm{TR}^2\right)-\left(0.0000173*\mathrm{AFR}^2\right) \\ & +\left(0.000844*\mathrm{AMS}^2\right) \end{aligned} \tag{12}$$

3.5.3 Model Equation for Al6063 + 10%B_4C + 5%$ZrSiO_4$

$$\begin{aligned} R_a = {} & +27.53858-(0.008183*\mathrm{WP})-(0.00894*\mathrm{TR}) \\ & -(0.016226*\mathrm{AFR})-(0.37177*\mathrm{AMS}) \\ & +(0.000010*\mathrm{WP}*\mathrm{TR})+(0.000023*\mathrm{WP}*\mathrm{AFR}) \\ & +(0.000088*\mathrm{WP}*\mathrm{AMS}) \\ & +(0.000035*\mathrm{TR}*\mathrm{AFR}) \\ & +(0.0000450*\mathrm{TR}*\mathrm{AMS}) \\ & +(0.0000136*\mathrm{AFR}*\mathrm{AMS})-\left(0.00002463*\mathrm{WP}^2\right) \\ & -\left(0.000049*\mathrm{TR}^2\right)+\left(0.000011*\mathrm{AFR}^2\right) \\ & +\left(0.001595*\mathrm{AMS}^2\right) \end{aligned} \tag{13}$$

3.5.4 Model Equation for Al6063 + 15%B_4C + 5%$ZrSiO_4$

$$\begin{aligned} \mathrm{Ra} = {} & +23.52340+(0.00518*\mathrm{WP}) \\ & +(0.013309*\mathrm{TR})-(5.10483\mathrm{E}*\mathrm{AFR}) \\ & -(0.37307*\mathrm{AMS})+(0.00000037*\mathrm{WP}*\mathrm{TR}) \\ & +(0.000011*\mathrm{WP}*\mathrm{AFR})-(0.00000033*\mathrm{WP}*\mathrm{AMS}) \\ & +(0.000025*\mathrm{TR}*\mathrm{AFR})-(0.00022*\mathrm{TR}*\mathrm{AMS}) \\ & -(0.000026*\mathrm{AFR}*\mathrm{AMS})-\left(0.000023*\mathrm{WP}^2\right) \\ & -\left(0.0000033*\mathrm{TR}^2\right)+\left(0.0000052*\mathrm{AFR}^2\right) \\ & +\left(0.00189*\mathrm{AMS}^2\right) \end{aligned} \tag{14}$$

3.6 Influence of Parameters on Al6063 Alloy and its Hybrid Composites for Ra

The interaction effect of AWJ cutting parameters for Ra on different materials is shown in Fig. 16. The response surface plots were made by using influencing factors in Al6063 alloy and its hybrid composites. These factors were attained from regression Eqs. (11)–(14). From these equations, it is noticed that abrasive mesh size and traverse rate for Al 6063 alloy, abrasive mesh size and flow rate for Al6063/5%B_4C/5%$ZrSiO_4$, Al6063/10%B_4C/5%$ZrSiO_4$, and Al6063/15%B_4C/5%$ZrSiO_4$. Likewise, the influencing factors combinations were obtained from the response surface plots. These combinations were selected based on the lower surface

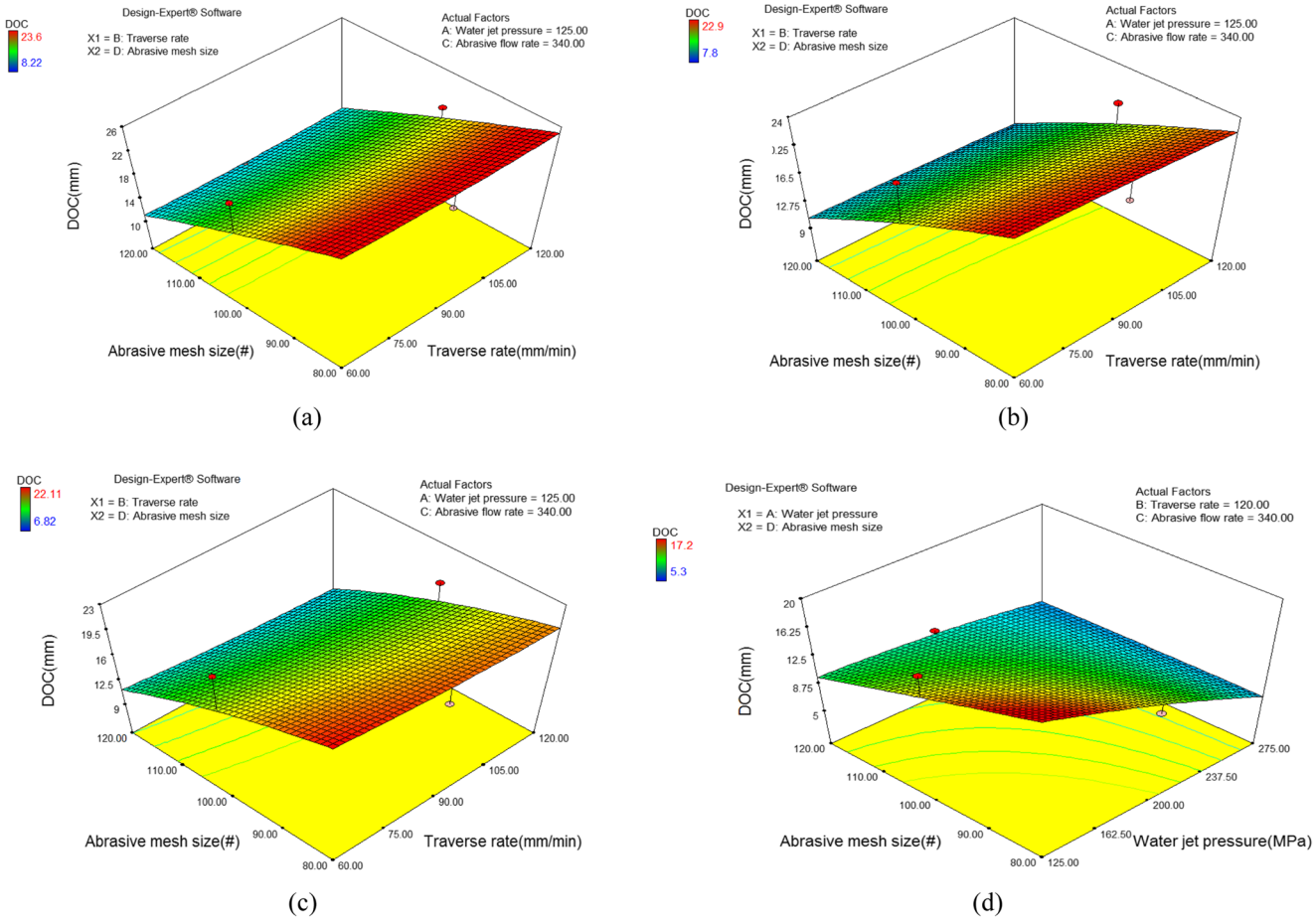

Fig. 10 Effect of significant factors on DOC with different materials. **a** Al6063 **b** Al6063 + 5%B_4C + 5%$ZrSiO_4$ **c** Al6063 + 10%B_4C + 5%$ZrSiO_4$ **d** Al6063 + 15%B_4C + 5%$ZrSiO_4$

roughness values. The significant factors and its combinations for Ra are shown in Table 18. From the results, it is revealed that different parameter combinations were found for obtaining lower surface roughness in different materials.

From Table 18, it is observed that by increasing the percentage of B_4C particles with Al6063/5%$ZrSiO_4$ increases the surface roughness. This result was made due to the reduction in cutting energy of the AWJ while machining aluminium hybrid composites. Surface roughness was also increased due to the upward deflection of AWJ [33]. Also, the reinforcement particles were dislodged and fractured from their location due to the brittle fracture (Fig. 14). Surface roughness was increased to 5.768 μm not only due to the brittle fracture and incomplete removal of matrix phase. It is also increased by the contamination of abrasives and reinforcement particles in the machined surfaces. Severity of this formation was also found in 15% of B_4C with Al6063/5%$ZrSiO_4$, as shown in Fig. 14. However, a lower roughness of 3.655 μm was attained at water jet pressure of 275 MPa, traverse rate of 90 mm/min, abrasive flow rate of 240 g/min and mesh size of #100. This level of settings produced a strong erosion process for the uniform cutting of hard and soft phases of the hybrid composite. As an outcome, a lower roughness was obtained. And, the absence of abrasive and reinforcement particle projections in the Al6063 alloy leads to a lower surface roughness, and this result was confirmed by the eroded surface, as shown in Fig. 13.

It is also observed that common parameter settings were found in 10% and 15% of B_4C with Al6063/5%$ZrSiO_4$. This was attributed to the increment of B_4C more than 5% needs the huge kinetic energy with uniform cutting action for the production of lower surface roughness. It was obtained by an employment of appropriate level of process parameter settings. From Table 18, it is concluded that abrasive mesh size was the most influencing factor for decreasing the surface roughness in Al6063 alloy and its hybrid composites. Finer grade of abrasive particles (#100 & #120) leads to increase the surface quality of materials. It is also observed that by increasing the percentage of hard reinforcements abrasive mesh size of #100 plays a vital role in surface roughness. This mesh size contains both

Table 8 Significant process parameters and its combinations for DOC

Types of Materials	Influencing process parameters	Process parameters combinations				DOC, mm
		P, MPa	TR, mm/min	AFR, g/min	AMS (#)	
Al 6063 alloy	AMS & TR	125	120	340	80	23.90
Al6063 + 5%B_4C + 5%$ZrSiO_4$	AMS & TR	125	120	340	80	22.90
Al6063 + 10%B_4C + 5%$ZrSiO_4$	AMS & TR	125	120	340	80	20.89
Al6063 + 15%B_4C + 5%$ZrSiO_4$	AMS & WP	125	120	340	80	17.20

sharper and finer edges as shown in Fig. 7(b). As a corollary, this kind of abrasives removes the material with fine surface irregularities. This result produced due to the uniform cutting of particle reinforced composites by the employment of abrasive mesh size #100. The further increment or decrement in abrasive mesh size (> or < #100) leads to decrease the energy required for machining hybrid composites with better surface finish.

3.7 Influence of the Various Reinforcement Percentage of 3D Topography

Figure 17 shows the machined surface topography for Al6063 alloy and their hybrid metal matrix composites. In this study, surface topography was examined with lower surface roughness of AWJ machined surfaces. The lower roughness values were found under different processing conditions. The maximum height of peak to the valleys (Pt), surface roughness (Sa), Skewness (Ssk) and kurtosis (Sku) were considered as roughness quality parameters in the present work.

Among the various topography profiles, Al6063 showed a lower surface roughness of 4.49 μm. Hybrid composites produced rough surfaces as the hard reinforcement particles restrict the uniform shearing action in the work material. The condition of the surface is confirmed by various surface roughness parameters. It is found that Al6063 alloy contain better surface topography features (lower Pt, and Sa) than other materials. This roughness array profile showed the fine irregularities in the machined surface compared to others. However, few peaks existed and randomly distributed on the cut surface. It is confirmed by Ssk and Sku values. Among different processing conditions, the better surface texture was obtained due to the employment of water jet pressure of 200 MPa, traverse rate of 90 mm/min, abrasive flow rate of 240 g/min and mesh size of #120. This finer grade abrasive restricts the formation of deeper peaks and valleys in Al 6063 alloy, is shown in Fig. 17a.

It is also noticed that the hybrid composites maintain the uniform distribution of peaks and valleys in the surface, and is confirmed by Ssk and Sku values. Texture profiles (size and distribution of peaks and valleys) were varied in hybrid composites. These textures were obtained by different process parameters settings. Parameter settings were varied due to the presence of reinforcement particles and its volume in the matrix phase. It is also observed that Al6063/15%B_4C/5%$ZrSiO_4$ exhibited a lower Ssk value which is lower than zero. Further, it confirms that number of peaks was limited nearby the valleys, and it is confirmed by 3D surface profile. It was seen that density of peaks (red) were less, however, its distribution was composed nearby the valleys, which is produced through a brittle fracture (craters) of reinforcement phases. It happens as this hard phase redirects and disperses the AWJ, and subsequently, peaks were formed and confined nearby the valleys. The results also revealed that all material surfaces showed a negative sign of Ssk. This confirmed that AWJ machine tool produced a non-uniform mixing of abrasives with water jet. This type of jet characteristics usually

Table 9 ANOVA for response surface quadratic model of MRR-Al6063

Source	Sum of Squares	Dof	Mean Square	F Value	*p* value Prob > F
Model	2.993E+006	14	2.138E+005	13.39	< 0.0001
Residual	2.236E+005	14	15,969.8		
Lack of Fit	2.229E+005	10	22,290.41	132.30	0.0001
Pure Error	673.96	4	168.49		
Cor Total	3.216E+006	28			
Std. Dev.	126.37	R-Squared	0.9305		
Mean	957.69	Adj R-Squared	0.8610		
C.V. %	13.20	Pred R-Squared	0.6005		
PRESS	1.285E+006	Adeq Precision	13.675		

Table 10 ANOVA for response surface quadratic model of MRR - Al6063 + 5%B_4C + 5%$ZrSiO_4$

Source	Sum of Squares	Dof	Mean Square	F Value	*p* value Prob > F
Model	2.529E+006	14	1.806E+005	6.05	0.0009
Residual	4.182E+005	14	29,874.89		
Lack of Fit	4.158E+005	10	41,584.28	69.14	0.0005
Pure Error	2405.70	4	601.42		
Cor Total	2.947E+006	28			
Std. Dev.	172.84	R-Squared	0.8581		
Mean	885.72	Adj R-Squared	0.7161		
C.V. %	19.51	Pred R-Squared	0.1859		
PRESS	2.399E+006	Adeq Precision	9.310		

forms the surface texture with a randomized distribution of peaks. In addition, Sku value of different material surfaces was found to be greater than 3 [34]. This parameter measures the number of peaks or valleys formed in the machined surface. The lower value was found in Al6063 alloy. Similarly, a higher Sku was found inAl6063/15%B_4C/5%$ZrSiO_4$. It indicates that ductility of the material was favorable for the uniform projection of peaks/valleys. Moreover, the hybrid composites do not allow the severe valleys on its surface by the reinforcement particles, is confirmed by a higher Sku value. This is also established that the rich content of reinforcement phase in the matrix surface had higher peaks with an absence of frequent valleys by AWJ. However, the deeper valleys were observed in hybrid composites. It is confirmed by a roughness array profile in Fig. 17d. This result happened by the inclusion of reinforcement particles in the matrix phase produced deeper valleys through a formation of craters by the detachment of reinforcement particles. The maximum deeper valley is found in Al6063/15%B_4C/5%$ZrSiO_4$. It might have happened through a poor bonding of reinforcement with matrix phases as more percentage of B_4C particles.

Also, it is noticed that the Pt value was higher than other materials with increase of the percentage of B_4C particles with 5% $ZrSiO_4$/Al6063. This was attributed to the detachment of reinforcement particles from the matrix phase. As a result, maximum height of peak to valley was formed in the machined surface. The higher value of Pt was also obtained as the incomplete removal of material from the hard phase may lead to protrude as peaks from the surface. This showed the lower machinability of process with Al6063/15%B_4C/5%$ZrSiO_4$. It is also confirmed that 10% and 15%B_4C with Al6063/5%$ZrSiO_4$ composites had lower frequency of fine irregularities than other materials which results in poor surface texture and is confirmed by Ssk and Sku. This result was found due to the increment in reinforcement particles along with the intrinsic feature of abrasives distribution in the AWJ.

3.8 Influence of the Various Reinforcement Percentage on Surface Morphology

The AWJ machined surfaces were examined with help of SEM images is shown in Fig. 18. In this study, SEM

Table 11 ANOVA for response surface quadratic model of MRR - Al6063 + 10%B_4C + 5%$ZrSiO_4$

Source	Sum of Squares	Dof	Mean Square	F Value	*p* value Prob > F
Model	2.551E+006	14	1.822E+005	13.02	< 0.0001
Residual	1.958E+005	14	13,988.04		
Lack of Fit	1.948E+005	10	19,482.80	77.58	0.0004
Pure Error	1004.56	4	251.14		
Cor Total	2.747E+006	28			
Std. Dev.	118.27	R-Squared	0.9287		
Mean	849.53	Adj R-Squared	0.8574		
C.V. %	13.92	Pred R-Squared	0.5908		
PRESS	1.124E+006	Adeq Precision	13.456		

Table 12 ANOVA for response surface quadratic model of MRR of Al6063 + 15%B_4C + 5%$ZrSiO_4$

Source	Sum of Squares	Dof	Mean Square	F Value	*p* value Prob > F
Model	1.209E+006	14	86,330.16	6.71	0.0005
Residual	1.802E+005	14	12,874.29		
Lack of Fit	1.759E+005	10	17,590.26	16.22	0.0081
Pure Error	4337.55	4	1084.39		
Cor Total	1.389E+006	28			
Std. Dev.	113.46	R-Squared	0.8702		
Mean	666.48	Adj R-Squared	0.7404		
C.V. %	17.02	Pred R-Squared	0.2656		
PRESS	1.020E+006	Adeq Precision	9.752		

analysis was taken on the machined surfaces with lower surface roughness conditions. These results were obtained by different cutting process parameters. From the results, it is observed that abrasive mesh size #120 was favorable for Al6063 alloy and mesh size #100 was favorable for hybrid composites. The other cutting

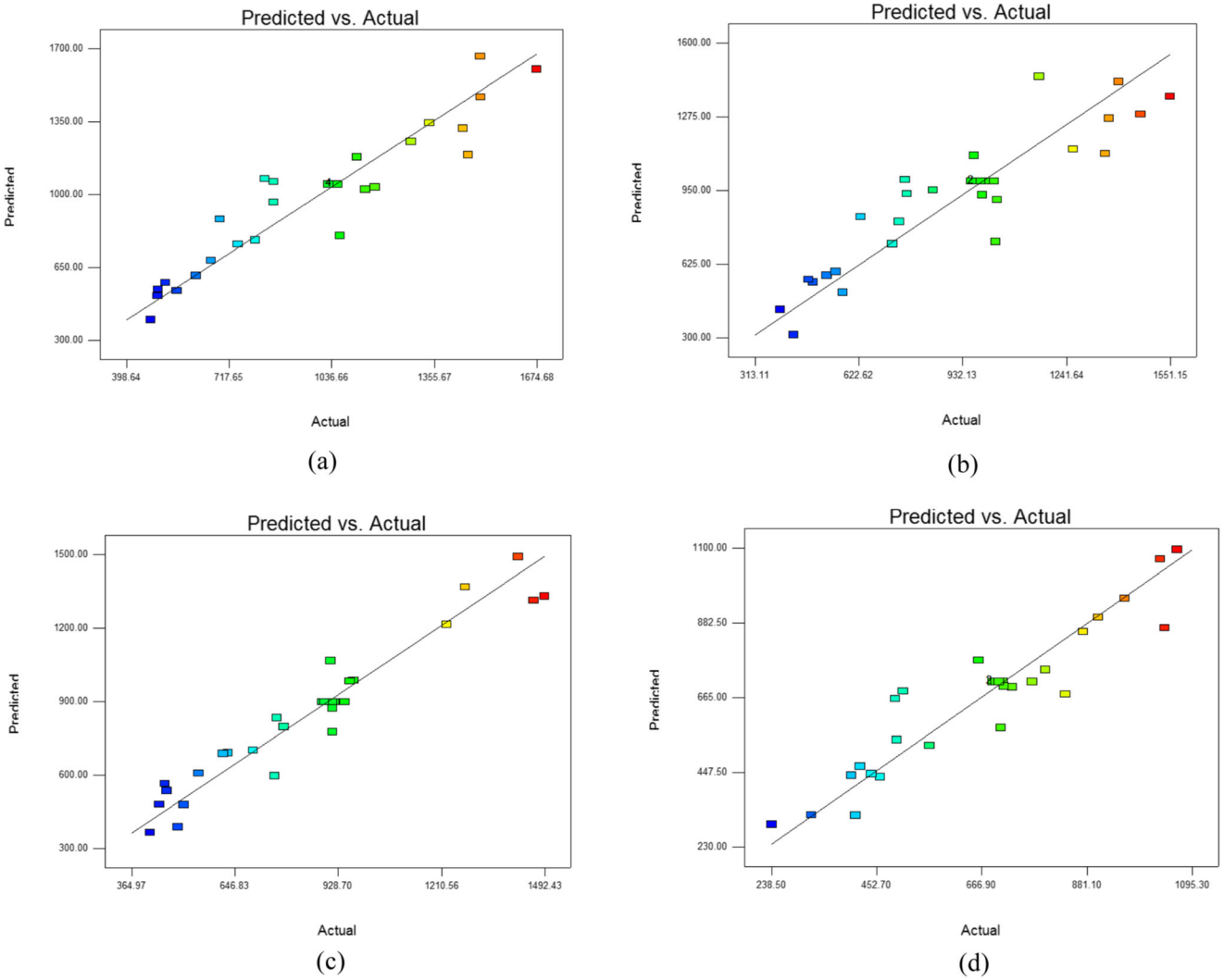

Fig. 11 Comparison between predicted and experimental value. **a** Al6063 **b** Al6063 + 5%B_4C + 5%$ZrSiO_4$ **c** Al6063 + 10%B_4C + 5%$ZrSiO_4$ **d** Al6063 + 15%B_4C + 5%$ZrSiO_4$

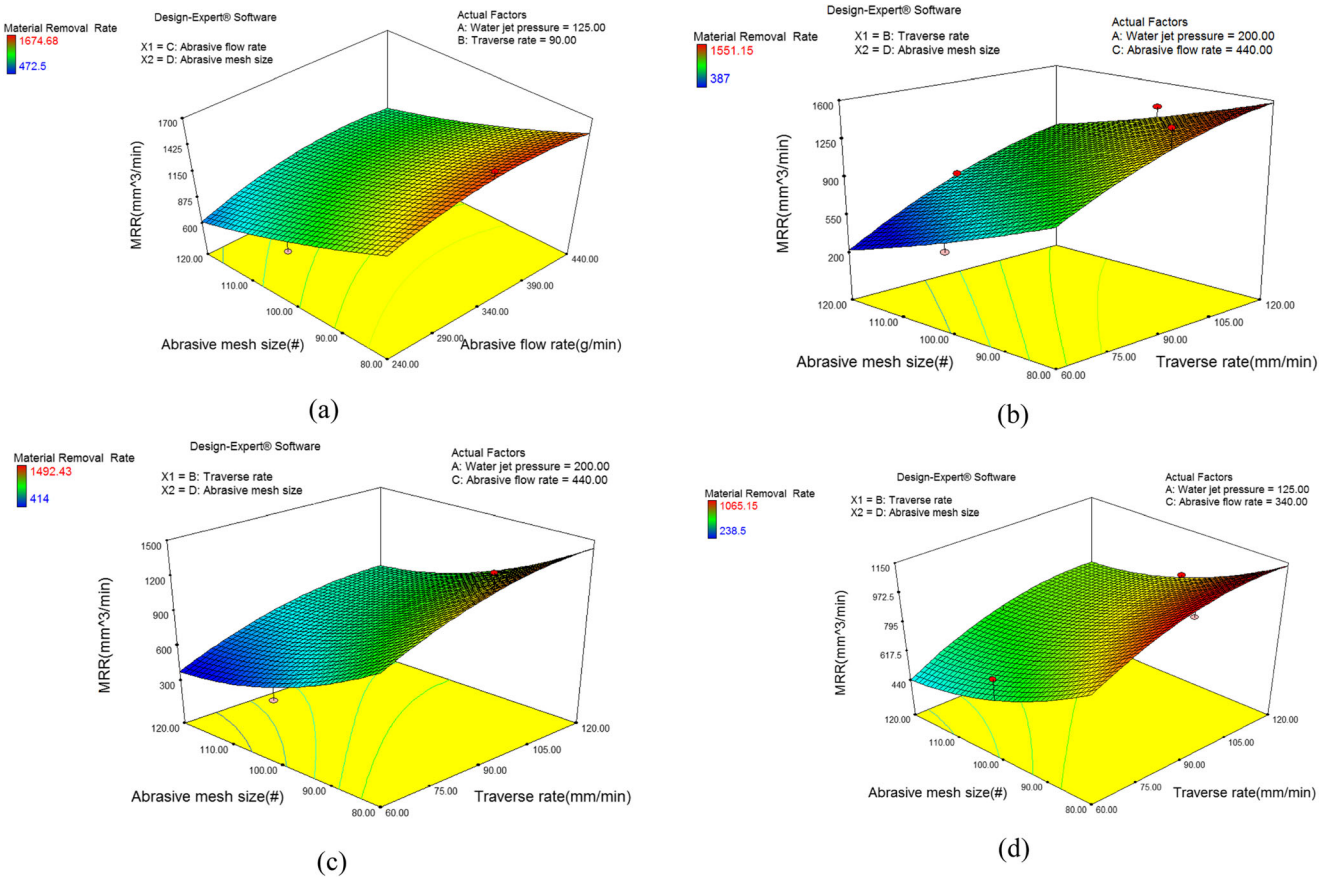

Fig. 12 Effect of significant factors on MRR with different materials. **a** Al6063 alloy **b** Al6063 + 5%B_4C + 5%$ZrSiO_4$ **c** Al6063 + 10%B_4C + 5%$ZrSiO_4$ **d** Al6063 + 15%B_4C + 5%$ZrSiO_4$

parameters were found at different levels. These results were observed due to the ductility and hardness of the materials. It is attributed to the account of reinforcement particles in Al6063 alloy.

In this study, SEM analysis was performed with different magnifications such as500X, 1000X.In this study, the SEM images were taken at top cutting region of the machined surfaces. From the results, it is noticed that wear tracks were occurs in Al6063 alloy and HMMCs. This form of wear tracks confirmed that material cutting action happened through a ductile erosion process. This erosion mechanism was further confirmed by formation of lips, and grooves [15]. It indicates that material removal occurs through the cutting wear and deformation wear modes. From the machined surfaces, it is revealed that cutting wear plays a crucial role in material removal process through a shearing action even though hybrid

Table 13 Significant process parameters and its combinations for MRR

Types of Materials	Influencing process parameters	Process parameters combinations				MRR, mm^3/min
		P, MPa	TR, mm/min	AFR, g/min	AMS, #	
Al 6063 alloy	AMS & AFR	125	90	440	80	1670
Al6063 + 5%B_4C + 5%$ZrSiO_4$	AMS &TR	200	120	440	80	1580
Al6063 + 10%B_4C + 5%$ZrSiO_4$	AMS & TR	200	120	440	80	1450
Al6063 + 15%B_4C + 5%$ZrSiO_4$	AMS & TR	125	120	340	80	1140

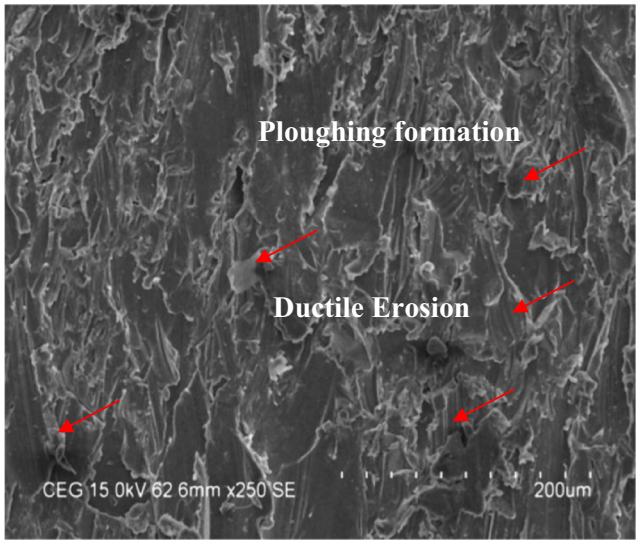

Fig. 13 Eroded surface of Al6063 alloy

composites were used. Also, brittle fracture was observed in HMMCs due to the presence of ceramic particles. Due to this, machined surfaces appeared as a rough morphology with similar contamination effects. The particles including reinforcements and abrasives were present on the machined surfaces. For all materials, wear tracks were erratically orientated in the surfaces. It has occurred due to the randomized distribution of abrasives in the high velocity water jet. It is also noticed that Al6063 alloy contains severe form of wear tracks and ploughing morphology in their surfaces. In addition to this, deep wear tracks were observed on the surfaces by the strong cutting action of single coarse abrasive grain. This causes the formation of lips adjoining with the grooves. From these observations, it is noticed that erosion process was rigorous in

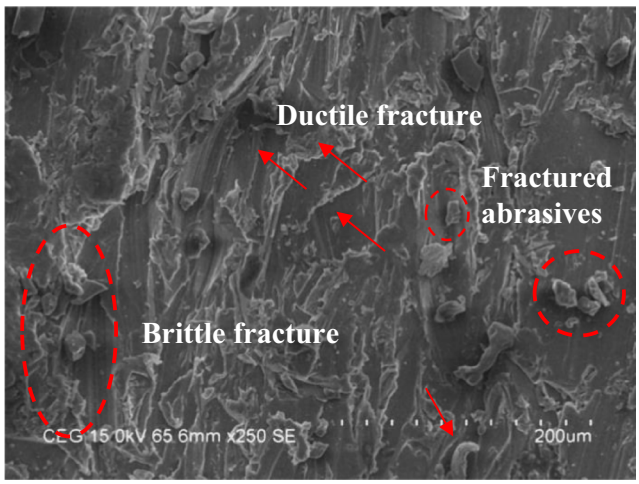

Fig. 14 Eroded surface of Al6063/15%B_4C/5%$ZrSiO_4$

Al6063 alloy due to its soft condition in absence of reinforcements.

It is also noticed that ductile mode of wear tracks was absent in Al6063/10%B_4C/5%$ZrSiO_4$ and Al6063/15%B_4C/5%$ZrSiO_4$. This result found owing to the presence of hard reinforcements in the base material. This resists the severe ploughing action through an increment in hardness and decrement in ductility of the matrix phase by hard reinforcement particles. Few regions of the surface in Al6063/10%B_4C/5%$ZrSiO_4$ revealed that grooves were produced through the abrasion process. This mechanism occurs through the bombardment of abrasives with hard reinforcement particles. As a result, deep groove was formed by the displacement of reinforcement particles, as shown in Fig. 18. Matrix phase was displaced to the side of the grooves, which it's also confirms the occurrence of abrasive wear. This allows the severe ploughing action through a pelting of reinforcement particles by the involvement of coarse abrasive grains in abrasive mesh size #100. Major contamination such as craters, tiny particles (fractured reinforcement particles and abrasives) and wear tracks were not seen in Al6063/5% $ZrSiO_4$ reinforced with 10% B_4C as it might be containing higher fracture toughness than other HMMCs. The fractured reinforced particles also indicate that the occurrence of abrasive wear mechanism due to inclusion of B_4C particles in the matrix phase. It is confirmed by the previous researchers [6, 7], one of the researchers found the maximum toughness with 10% weight of B_4C [7]. Despite this, B_4C particle was projected on the surface due to the partial pullout of it. Particle confirmation was done by elemental composition analysis.

Distinct surfaces were also observed due to the occurrence of brittle fracture in reinforcement phase along with the ductile erosion process [2]. It is confirmed by the dark spots (craters)in SEM images of Al6063/5%$ZrSiO_4$ reinforced with 5% B_4C and 15% B_4C. The continuous form of shallow cavities with wrinkled particles were seen in SEM image at a magnification of 500x is shown in Fig. 18. This type of cavity was produced due to the lack of interfacial bonding between the reinforcements with matrix phase. Reinforcement particles were dislodged from the matrix phase not only by brittle fracture and pelting of abrasives. Particle detachments also increased by reduction in fracture toughness and increment in hardness of the HMMCs. This reduction may happen due to the increment in weight fraction of ceramic particles in the base material. In view of this, tinier fractured and pull out of reinforced grains were seen in Al6063/5%B_4C/5%$ZrSiO_4$ and Al6063/

Table 14 ANOVA for response surface quadratic model of R_a - Al6063

Source	Sum of Squares	Dof	Mean Square	F Value	*p* value Prob > F
Model	3.72	14	0.27	9.44	< 0.0001
Residual	0.39	14	0.028		
Lack of Fit	0.27	10	0.027	0.85	0.6225*
Pure Error	0.13	4	0.032		
Cor Total	4.12	28			
Std. Dev.	0.17	R-Squared	0.9042		
Mean	2.62	Adj R-Squared	0.8085		
C.V. %	6.4	Pred R-Squared	0.5771		
PRESS	1.74	Adeq Precision	11.797		

*Insignificant

15%B_4C/5%$ZrSiO_4$ machined surfaces. It is also noticed that wear tracks were not found due to the influence of hardness by rich particles of B_4C (>10%) with 5%$ZrSiO_4$ in Al6063 alloy even though higher and lower abrasive flow rates were employed. However, a single large size abrasive was stick with the Al6063/15%B_4C/5%$ZrSiO_4$, is seen in the SEM image with higher magnification in Fig. 18. Abrasive was confirmed by the coarser edges of the grain. Also, the fractured tiny particles were deposited in the deep craters. This type of crater was formed due to the decrement in impact resistance of the composite by a higher weight fraction of B_4C particles. Deep crater was also formed by the total detachments of reinforcement particles from the matrix phase because of the weak interfacial bond of reinforcement with the matrix phase. It is also noticed that tearing was formed by the end of brittle fracture in HMMCs.

In addition, large size particle contaminations were not seen in Al6063/5%B_4C/5%$ZrSiO_4$ and Al6063 alloy. Even though, a small size of abrasive particles was embedded in the cut surface, which is confirmed by the presence of Si particles [32–34]. It was measured by using EDS technique. This contamination was formed through a production and improper removal of an embedment of fractured $ZrSiO_4$ and garnet abrasives in the machined surface. Particle contamination is greatly reduced by increasing hardness of the Al6063 alloy through an increment in weight fraction of B_4C particles with $ZrSiO_4$ in the matrix phase of metal. By claiming of this, a large percentage of Si particles were observed in Al6063/5%B_4C/5%$ZrSiO_4$ and Al6063/15%B_4C/5%$ZrSiO_4$, as shown in Table 19. From Table 19, it is noticed that lower contamination was found in Al6063/10%B_4C/5%$ZrSiO_4$. This result happened due to the absence of cavities by the improvement in fracture toughness of the composite by 10% of B_4C.

In Al6063/5%$ZrSiO_4$ reinforced with 5%B_4C produced a higher contaminated surface in which crushed particles and abrasives were severely deposited in the

Table 15 ANOVA for response surface quadratic model of R_a - Al6063+ 5%B_4C + 5%$ZrSiO_4$

Source	Sum of Squares	Dof	Mean Square	F Value	*p* value Prob > F
Model	4.92	14	0.35	8.42	0.0001
Residual	0.58	14	0.042		
Lack of Fit	0.28	10	0.028	0.37	0.9075*
Pure Error	0.3	4	0.076		
Cor Total	5.51	28			
Std. Dev.	0.2	R-Squared	0.8939		
Mean	3.65	Adj R-Squared	0.7877		
C.V. %	5.6	Pred R-Squared	0.6199		
PRESS	2.09	Adeq Precision	9.703		

*Insignificant

Table 16 ANOVA for response surface quadratic model of R_a - Al6063 + 10%B_4C + 5%$ZrSiO_4$

Source	Sum of Squares	Dof	Mean Square	F Value	*p* value Prob > F
Model	6.93	14	0.5	6.07	0.0009
Residual	1.14	14	0.082		
Lack of Fit	1.08	10	0.11	6.79	0.04
Pure Error	0.064	4	0.016		
Cor Total	8.07	28			
Std. Dev.	0.29	R-Squared	0.8585		
Mean	4.06	Adj R-Squared	0.717		
C.V. %	7.03	Pred R-Squared	0.2181		
PRESS	6.31	Adeq Precision	8.187		

cavities. Even though, a higher hardness of Al6063/5%$ZrSiO_4$ reinforced with 15% of B_4C produced cavities by a strong brittle fracture in the reinforcement phases in which crushed particles were embedded. From this result, an impact resistance was decreased by increasing the weight of reinforcement particles. It is observed that higher influence of reinforcements may lead to produce the rough morphology (lip formation) and contaminated surface (fractured grains). These results occur as an increment in weight fraction of B_4C with $ZrSiO_4$ particles in Al6063 decreases the cutting ability of AWJ, and yield the surface with incomplete removal of chips, and fractured and detached particles, which were noted in Al6063/15%B_4C/5%$ZrSiO_4$. The enlarged section is shown in Fig. 18 by a red square box, in which the chip had a segmented shape. This kind of chips formed through a long shearing action. This was due to the difficulties in erosion by an insufficient energy of coarse abrasive grain with hybrid composites. It was confirmed that material removal occurs through a ductile fracture. Further, the machined surfaces require the cleaning operation so as to remove the fractured abrasives and reinforcement particles from the cut surfaces.

In view of surface deterioration, the previous studies were also reported with severe contamination i.e. abrasive embedment and reinforcement detachment in the AWJ machining of composites [17, 21, 25], which might be affect the fatigue life. Abrasive embedment is a characteristic of the AWJ process [15]. However, this contamination can be reduced by using ultrasonic cleaning and soluble abrasives. It is proved by Boud et al. [35] who studied on different materials such as brass, copper, steel and Inconel. Use of ultrasonic cleaning and soluble abrasives can be done in future work of this study.

4 Conclusions

In this study, machinability studies were carried out on different aluminium hybrid composites by using AWJ. Hybrid composites were developed by varying the percentage of B_4C (5%, 10% and 15%) with Al6063/

Table 17 ANOVA for response surface quadratic model of R_a - Al6063 + 15%B_4C + 5%$ZrSiO_4$

Source	Sum of Squares	Dof	Mean Square	F Value	*p* value Prob > F
Model	7.18	14	0.51	5.53	0.0014
Residual	1.3	14	0.093		
Lack of Fit	1.29	10	0.13	103.61	0.0002
Pure Error	4.99E-03	4	1.25E-03		
Cor Total	8.48	28			
Std. Dev.	0.3	R-Squared	0.8468		
Mean	4.25	Adj R-Squared	0.6936		
C.V. %	7.16	Pred R-Squared	0.12		
PRESS	7.46	Adeq Precision	7.253		

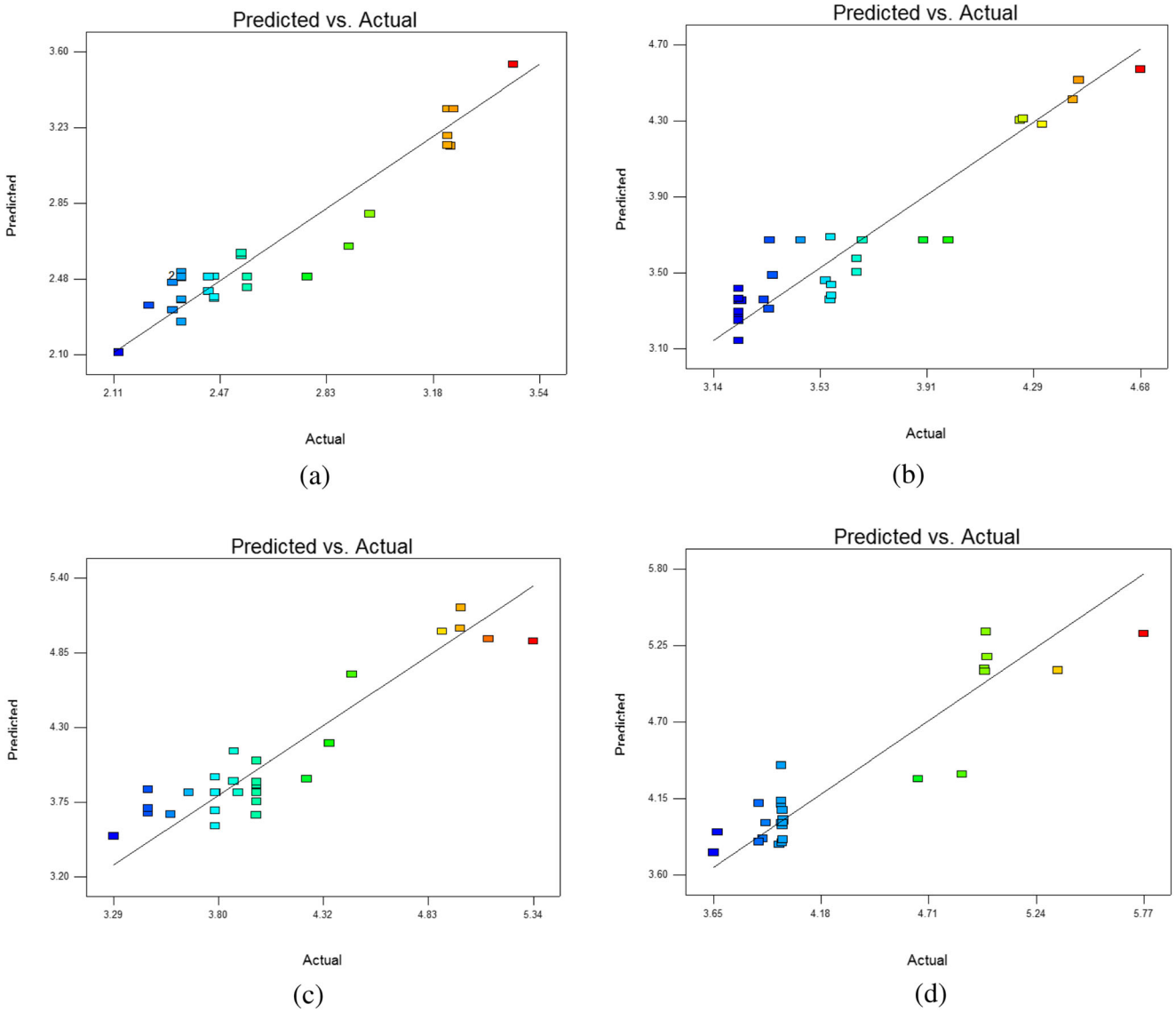

Fig. 15 Comparison between predicted and experimental value. **a** Al6063 **b** Al6063 + 5%B_4C + 5%$ZrSiO_4$ **c** Al6063 + 10%B_4C + 5%$ZrSiO_4$ **d** Al6063 + 15%B_4C + 5%$ZrSiO_4$

5%$ZrSiO_4$. In the present work, performance and surface characteristics were studied. And, the results are presented below.

4.1 Major Contribution

1. Depth of cut and material removal rate were found to be lower in hybrid composites compared to the Al6063 alloy. This happened due to increment in to hardness of the material by the inclusion of B_4C and $ZrSiO_4$ reinforcements in the base material. In hybrid composites, the higher depth of cut and material removal rate were observed at 5% B_4C with Al6063/5% $ZrSiO_4$. And, the values are found to be 22.90 mm and 1551.15 mm^3/min.
2. A lowest surface roughness of 2.13 μm was obtained in Al6063 alloy due to the uniform removal of material from the soft surface. Surface roughness values were increased by increasing the volume of reinforcements in the metal matrix constituent. The average roughness was found in the range of 3.234–5.345 μm.
3. Among cutting parameters, water jet pressure of 100 MPa and traverse rate of 120 mm/min were found suitable for

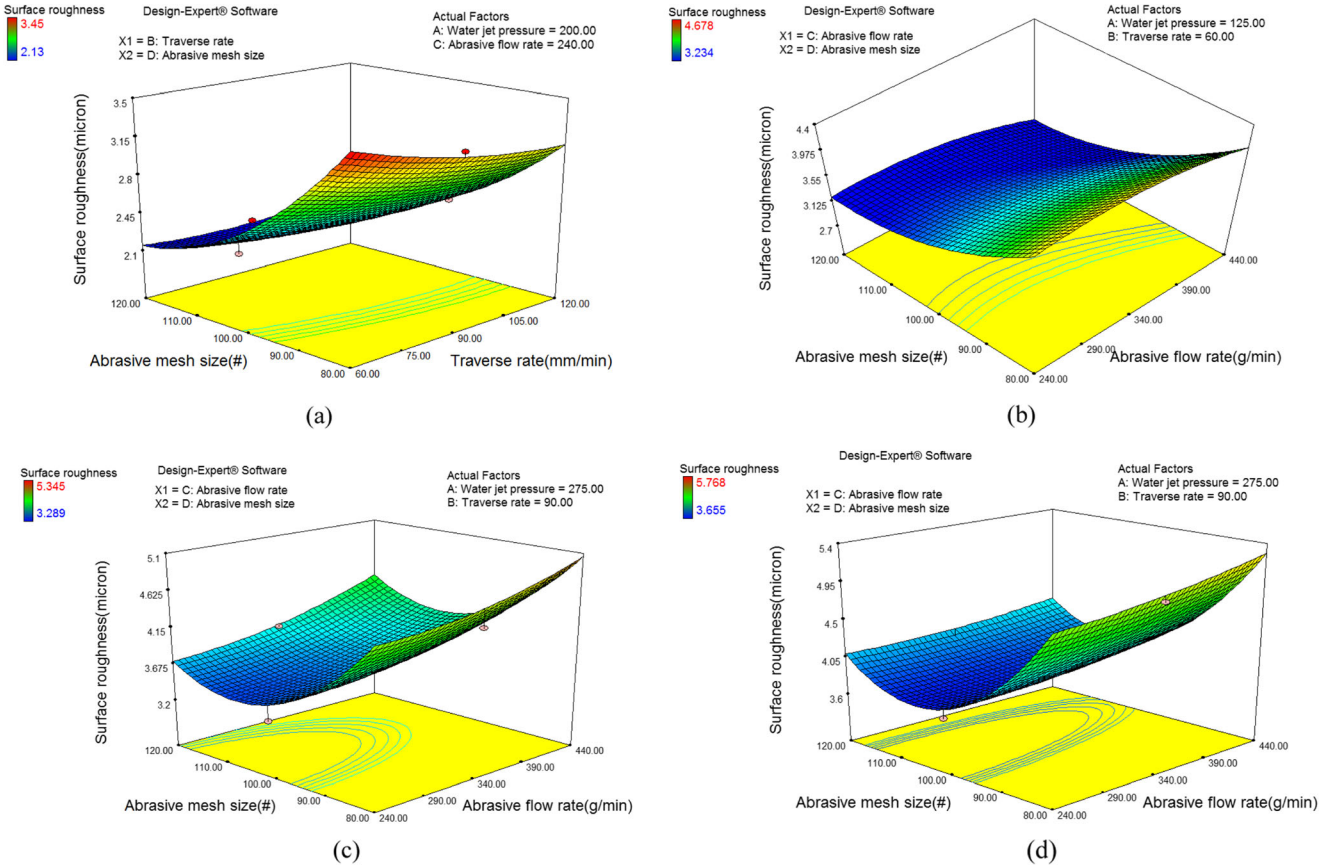

Fig. 16 Effect of significant factors on Ra with different materials. **a** Al6063 **b** Al6063 + 5%B_4C + 5%$ZrSiO_4$ **c** Al6063 + 10%B_4C + 5%$ZrSiO_4$ **d** Al6063 + 15%B_4C + 5%$ZrSiO_4$

machining aluminium hybrid composites with a higher depth of cut and material removal rate. In addition, the abrasive mesh size of #100 was the influencing factor for the production of a lower surface roughness in all types of hybrid composites.

4. A combined mode of ductile fracture and brittle fracture was seen in the machined hybrid composite surfaces. This was confirmed by the presence of wear tracks and craters in the machined surfaces. It was seen higher in 15% of B_4C with Al6063/5% of $ZrSiO_4$ hybrid composite.

Table 18 Significant process parameters and its combinations for Ra

Types of Materials	Influencing process parameters	Process parameters combinations				Ra, μm
		P, MPa	TR, mm/min	AFR, g/min	AMS, #	
Al 6063 alloy	AMS &TR	200	90	240	120	2.130
Al6063 + 5%B_4C + 5%$ZrSiO_4$	AMS &AFR	125	60	340	100	3.234
Al6063 + 10%B_4C + 5%$ZrSiO_4$	AMS& AFR	275	90	240	100	3.289
Al6063 + 15%B_4C + 5%$ZrSiO_4$	AMS &AFR	275	90	240	100	3.655

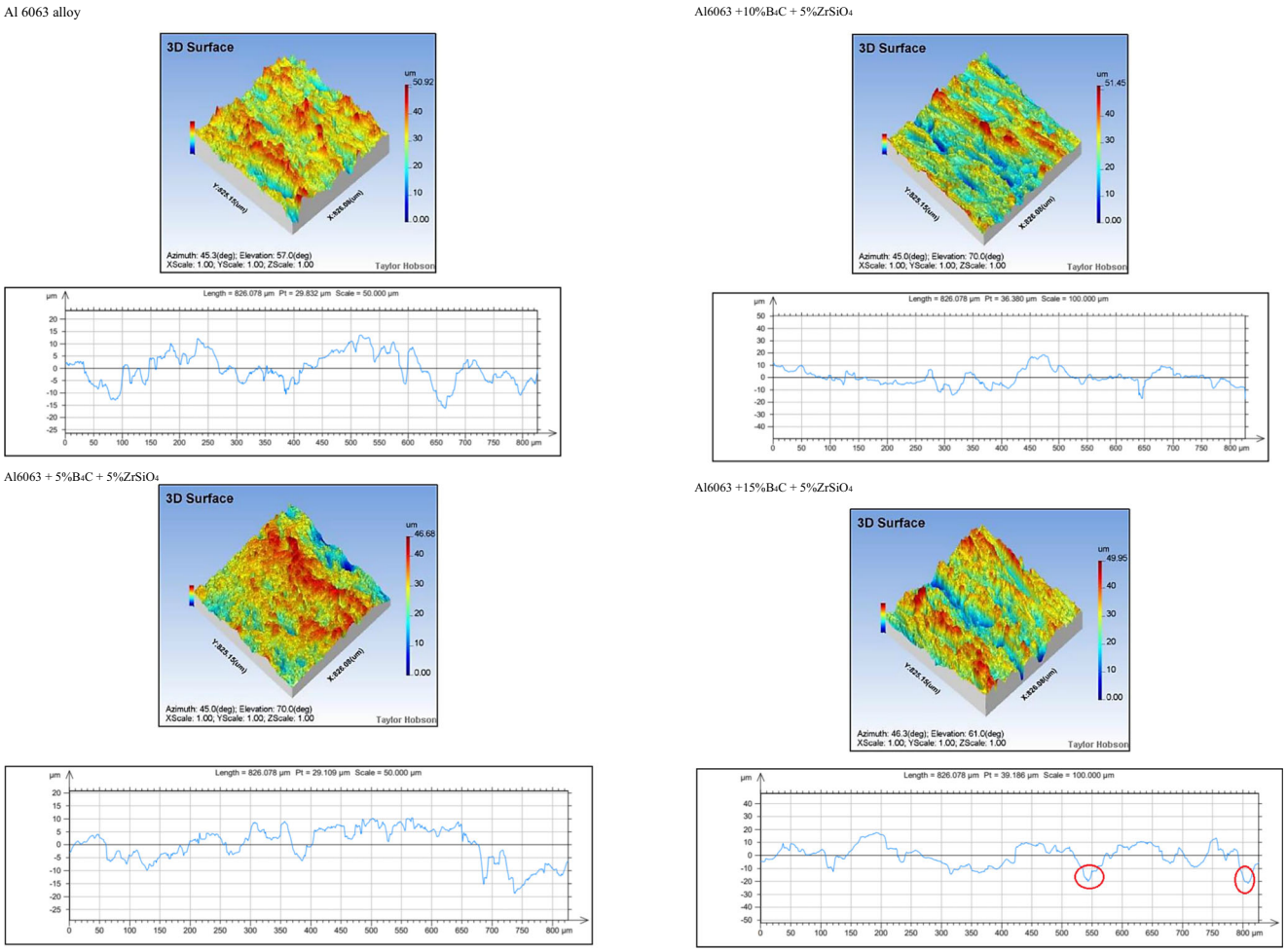

Fig. 17 3D surface topography of Al6063 alloy and HMMCs. **a** P 200 MPa; TR 90 mm/min; AFR 240g/min; AMS #120 **b** P 125 MPa; TR 60 mm/min; AFR 340g/min; AMS #100 **c** P 275 MPa; TR 90 mm/min; AFR 240g/min; AMS #100 **d** P 275 MPa; TR 90 mm/min; AFR 240g/min; AMS #100

5. Severe contamination (presence of fractured abrasives and reinforcement particles) was observed in Al6063/15% B_4C/5%$ZrSiO_4$. Surface of the kind was found due to the occurrence of deep craters through a detachment of more reinforcement particles by the pelting of abrasives.

4.2 Limitations

6. ANOVA results confirmed that the lack of fit for the depth of cut and material removal rate of HMMCs were found to be significant (<0.05). Similarly, the lack of fit for the surface roughness was found to be significant except Al6063/5%B_4C/5%$ZrSiO_4$.

7. Fragmented abrasives and particle detachments in the machined surfaces leads to deteriorate the surface quality of the hybrid composites. This kind of surfaces were found due to the occurrence of particle pull out by weak interfacial bonding of reinforcements with the matrix phase of metal, and decrement in impact resistance of HMMCs by increment in weight of B_4C particles.

4.3 Future Scope

8. It is further needed to select the narrow range of process parameters for the response variations. In future, the effect of Al_2O_3 & SiC abrasives with different

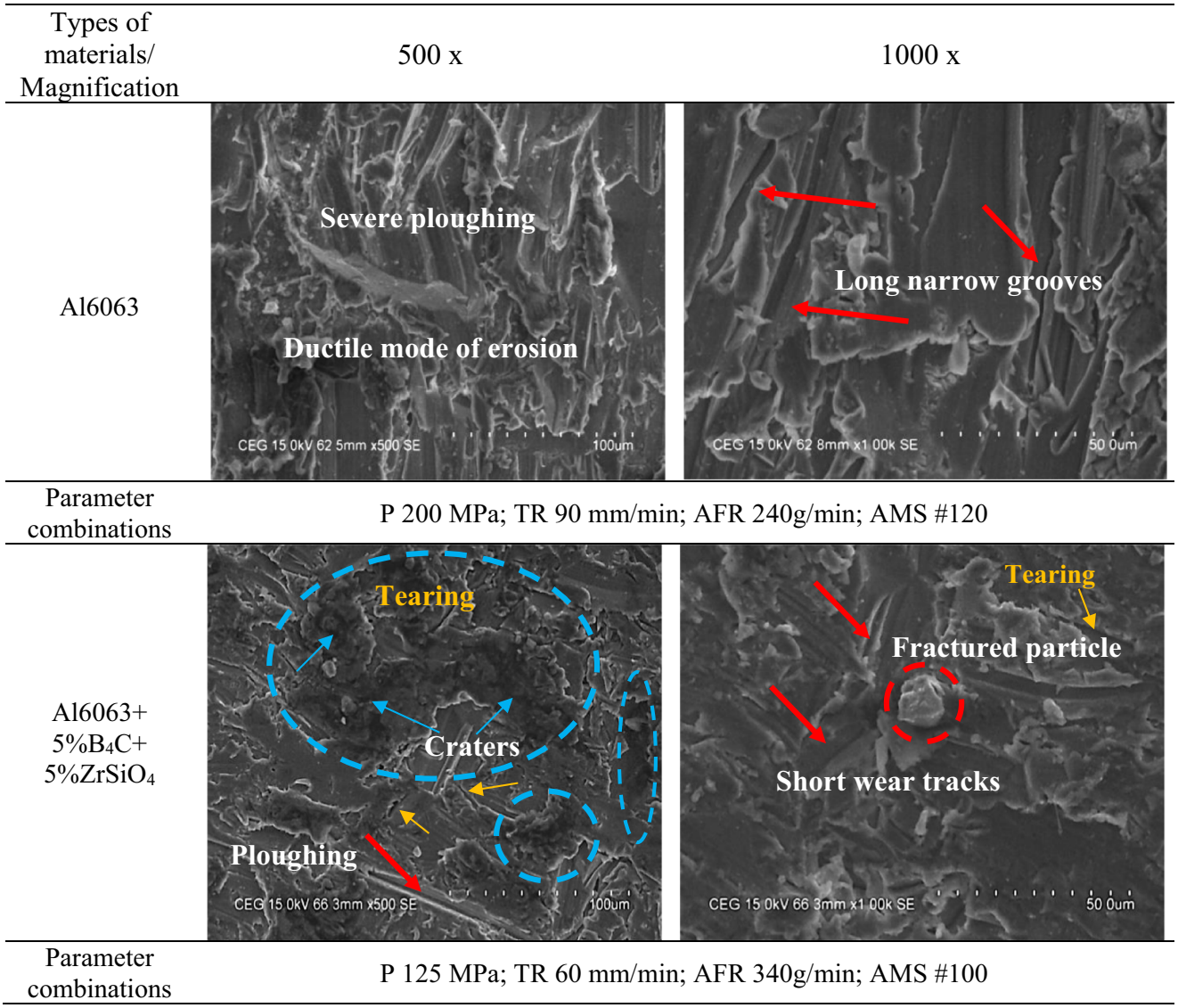

Fig. 18 Surface morphology of Al6063 and HMMCs

mesh sizes can be investigated on AWJ cutting of Al6063/B_4C/$ZrSiO_4$.

9. In view of surface quality, finer grade mesh sizes (>#120) of abrasives can be chosen for the enhancement of surface quality features. The conventional abrasives with ultrasonic oscillator and soluble type abrasives can also be recommended to minimize the contaminations like abrasive embedment and reinforcement detachment in the HMCCs surfaces.
10. As well, the cutting-edge metaheuristics techniques can be used for the generation of precise parameter settings for machining HMCCs.

Acknowledgments Authors acknowledge the M/s. Sivasakthi water jet cutting pvt ltd, Chennai for experimental support.

Author Contributions P. Thamizhvalavan – Conceptualization, Investigation, Software; N. Yuvaraj – Methodology, Writing-Original Draft & Review Editing; S. Arivazhagan – Validation, Supervision.

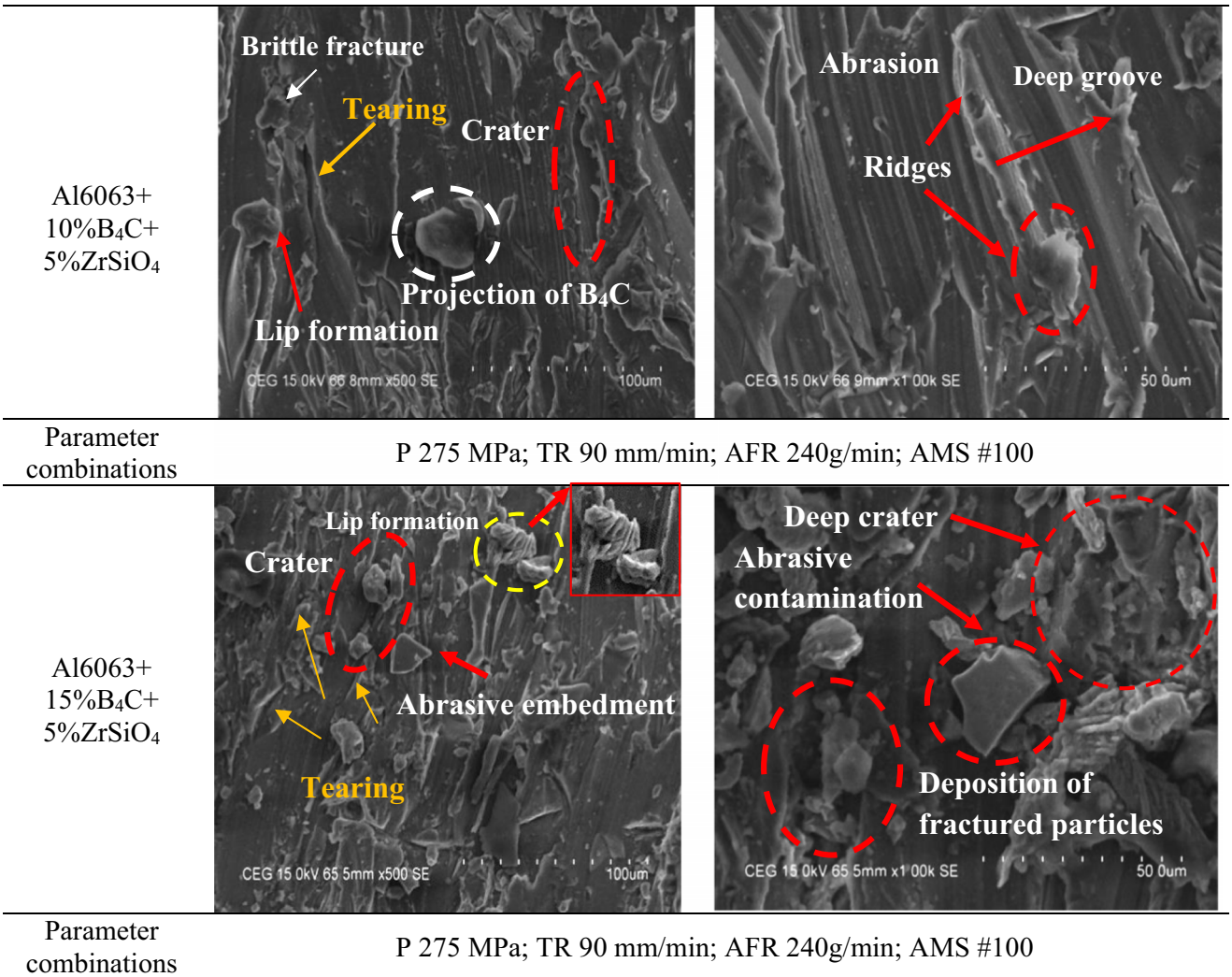

Fig. 18 continued.

Data Availability The datasets generated during the current study are available from the corresponding author on reasonable request.

Compliance with Ethical Standards

Conflict of Interest The authors have no conflicts of interest to declare that are relevant to the content of this article.

No humans and animals involved in this research work.

Consent to Participate Not applicable.

Consent for Publication Informed consent was obtained from all authors of this article for publication.

Table 19 Percentage of Si particles in the machined surfaces

S. No	Types of materials	% of Si particle		% of Contamination
		Before machining	After machining	
1	Al 6063 alloy	0.63	1.24	0.61
2	Al6063/5%B_4C/5%$ZrSiO_4$	1.73	2.72	0.99
3	Al6063/10%B_4C/5%$ZrSiO_4$	1.91	1.97	0.06
4	Al6063/15%B_4C/5%$ZrSiO_4$	2.20	2.61	0.41

References

1. Lalmuan SK, Das S, Chandrasekaran M, Tamang SK (2017) Machining investigation on hybrid metal matrix composites-review. Mater Today Proc 4(8):8167–8175
2. Umanath K, Palanikumar K, Selvamani ST (2013) Analysis of dry sliding wear behaviour of Al6061/SiC/Al_2O_3 hybrid metal matrix composites. Compos Part B 53:159–168
3. Rajmohan T, Palanikumar K, Prakash S (2013) Grey-fuzzy algorithm to optimise machining parameters in drilling of hybrid metal matrix composites. Compos Part B 50:297–308
4. Krishna MV, Xaviour AM (2014) An investigation on the mechanical properties of hybrid metal matrix composites. Procedia Eng 97: 918–924
5. Cao F, Chen C, Wang Z, Muthuramalingam T, Anbuchezhiyan G (2019) Effects of silicon carbide and tungsten carbide in Aluminium metal matrix composites. Silicon 11(6):2625–2632
6. Liu S, Wang Y, Muthuramalingam T, Anbuchezhiyan G (2019) Effect of B_4C and MOS_2 reinforcement on micro structure and wear properties of aluminum hybrid composite for automotive applications. Composites Part B 176:107329
7. Karabulut S, Karakoc H, Cıtak R (2016) Influence of B_4C particle reinforcement on mechanical and machining properties of Al6061/B_4C composites. Compos Part B 101:87–98
8. Arun KS, Pannerselvam T, Raghuraman S (2015) Study on Mechanical Properties of Aluminium Based Metal Matrix Composites by Hybrid Reinforcement. Appl Mech Mater 813–814:116–120
9. Saini VK, Khan ZA, Siddiquee AN (2012) Advancement in non-conventional machining of aluminum metal matrix composite materials. Int J Eng Res Technol 1(3):1–14
10. Satishkumar D, Kanthababu M, Vajjiravelu V, Anburaj R, Thrirumalai Sundarrajan N, Arul H (2011) Investigation of wire electrical discharge machining characteristics of Al6063/SiC_P composites. Int J Adv Manuf Technol 56(9–12):975–986
11. Sankar M, Gnanavelbabu A, Rajkumar K, Thushal N (2017) A electrolytic concentration effect on the abrasive assisted-electrochemical machining of aluminum-boron carbide composite. Mater Manuf Process 32(6):687–692
12. Ravindra NY, Vinod Y (2016) Machining of hybrid-metal matrix composite using Erosion-abrasion based compound wheel in electrical discharge grinding. Int J Particulate Sci Technol 35(4):494–504
13. Muller F, Monaghan J (2000) Non-conventional machining of particle reinforced metal matrix composite. Int J Mach Tools Manuf 40(9):1351–1366
14. Pramanik A (2014) Development in nontraditional machining of particle reinforcement metal matrix composites. Int J Machine Tool Manufact 86:44–61
15. Natarajan Y, Murugesan PK, Mohan M, Liyakath Ali Khan SA (2020) abrasive water jet machining process: a state of art of review. J Manuf Process 49:271–322
16. Santhanakumar M, Adalarasan R, Rajmohan M (2016) Parameter design for cut surface characteristics in abrasive waterjet cutting of Al/SiC/Al_2O_3 composite using grey theory based RSM. J Mech Sci Technol 30(1):371–379
17. Gnanavelbabu A, Rajkumar K, Saravanan P (2018) Investigation on the cutting quality characteristics of abrasive water jet machining of AA6061-B_4C-hBN hybrid metal matrix composites. Mater Manuf Process 33(12):1313–1323
18. Kumar KR, Sreebalaji VS, Pridhar T (2018) Characterization and optimization of abrasive water jet machining parameter of aluminum tungsten carbide composites. Measurement 117:57–66
19. Gnanavelbabu A, Saravanan P, Rajkumar K, Karthikeyan S, Baskaran R (2018) Effect of abrasive Waterjet machining parameters on hybrid AA6061-B_4C-CNT composites. Mater Today: Proc 5(2):13438–13450
20. Srivastava AK, Nag A, Dixit AR, Tiwari S, Scucka J, Zelenak M, Scucka J, Zelenak M, Hloch S, Hlavacek P (2017) Surface integrity in tangential turning of hybrid MMC A359/B_4C/Al_2O_3 by abrasive water jet. J Manuf Process 28(1):11–20
21. Sasikumar KSK, Arulshri KP, Ponappa K, Uthayakumar M (2018) A study on kerf characteristics of hybrid aluminum 7075 metal matrix composites machined using abrasive water jet machining technology. Proc Inst Mech Eng B J Eng Manuf 232(4):690–704
22. Metin K, Kanca E, Eyerciogiu O (2011) Prediction of surface roughness in abrasive water jet machining of particles reinforced MMCs using genetic expression programming. Int J Adv Manuf Technol 55:955–968
23. Mardi KB, Dixit AR, Mallick A, Pramanik A, Ballokova B, Hvizdos P, Foldyna J, Scucka J, Hlavacek P, Zelenak M (2017) Surface integrity of mg-based nano composite produced by abrasive water jet machining (AWJM). Mater Manuf Process 32(15): 1707–1714
24. Srinivas S, Ramesh BN (2012) Penetration ability of abrasive waterjet in cutting of aluminum silicon carbide particulate metal matrix composites. Int J Machin Sci Technol 16(3):337–354
25. Ramulu M, Raju SP, Inoue H, Zeng J (1993) Hydro abrasive erosion characteristics of 30vol.%SiCp/6061-T6 Al composites at shallow impact angle. Wear 166(1):55–63
26. Hamatani G, Ramulu M (1990) Machinability of high temperature composites by abrasive water jet. J Eng Mater Technol 112(4):381–386
27. Manoj M, Jinu GR, Muthuramalingam T (2018) Multi response optimization of AWJM process parameters on machining TiB_2 particles reinforced Al7075 composite using Taguchi-DEAR methodology. Silicon 10:2287–2293
28. Neusen KF, Rohatgi KP, Vaidyanathan C, Alberts D (1997) Abrasive water jet cutting of Metal Matrix Composites. In proc.4th U.S. Waterjet conference, Berkeley, pp 272–283
29. Savrun E, Taya M (1988) Surface characterization of SiC whisker/2124 aluminum and Al_2O_3 composites machined by abrasive water jet. J Mater Sci 23(4):1453–1458
30. Kumaran ST, Uthayakumar M, Mathiyazhagan P, Krishna Kumar K, Muthu KP (2015) Effect of abrasive grain size of the AWJM performance on AA6351-SiC-B4C hybrid composites. Appl Mech Mater 766–767:324–329
31. Srinivas S, Babu NR (2011) Role of garnet and silicon carbide abrasives in abrasive waterjet cutting of aluminum-silicon carbide particulate metal matrix composites. Int J Appl Res Mech Eng 1: 109–122
32. Yuvaraj N, Kumar MP (2017) Study and evaluation of abrasive water jet cutting performance on AA5083-H32 aluminum alloy by varying the jet impingement angles with different abrasive mesh sizes. Int J Mach Sci Technol 21(3):385–415
33. Kumaran ST, Jo Ko T, Uthayakumar M, Islam MM (2017) Prediction of surface roughness in abrasive water jet machining of CFRP composites using regression analysis. J Alloys Compd 724:1037–1045
34. Yuvaraj N, Kumar MP (2017) Surface integrity studies on abrasive water jet cutting of AISI D2 steel. Mater Manuf Process 32(2):162–170
35. Boud F, Murray JW, Loo LF, Clare AT, Kinnell PK (2014) Soluble abrasives for Waterjet machining. Mater Manuf Process 29(11–12): 1346–1352